Journal of Catalysis **207,** 166–182 (2002)
doi:10.1006/jcat.2002.3518, available online at http://www.idealibrary.com on IDEAL®

A DRIFTS Study of Cu–ZSM-5 Prior to and during Its Use for N_2O Decomposition

Paul E. Fanning[1] and M. Albert Vannice[2]

Department of Chemical Engineering, Pennsylvania State University, University Park, Pennsylvania 16802-4400

Received May 24, 2001; revised January 3, 2002; accepted January 3, 2002

Cu–ZSM-5 and Na–ZSM-5 were characterized by diffuse reflectance infrared Fourier transform spectroscopy (DRIFTS) prior to and during N_2O decomposition at various temperatures to learn more about the state of the Cu–ZSM-5 catalyst and to better understand its very high activity for this reaction. In addition to IR bands also exhibited by Na–ZSM-5, the spectrum of Cu–ZSM-5 at 300 K prior to any thermal treatment displayed an additional band between 900 and 1000 cm^{-1}, which was assigned to a stretching mode of an $Si–O^-$ bond perturbed by Cu^{2+} species as opposed to a similarly perturbed Si–O–Si or Si–O–Al zeolite vibration. Purging this sample in Ar at 300 K removed both adsorbed water and water coordinated in octahedral $[Cu(H_2O)_6]^{2+}$ complexes. Heating to 773 K resulted in the thermal reduction of Cu^{2+} to Cu^+, and a substantial fraction of the copper ions was stabilized as $Si–O^-Cu^+$. When N_2O was introduced to Cu–ZSM-5, transient bands were observed which were assigned to N_2O adsorbed on Cu^+ via the O atom. Only Cu–ZSM-5 exhibited a slight but rapid decrease in the 3597-cm^{-1} υOH band for bridging Si(OH)Al groups and it was accompanied by the appearance of a band near 910 cm^{-1}, indicating oxidation of Cu^+ to Cu^{2+}. No unequivocal bands for adsorbed N_2O were detected under steady-state decomposition conditions with any catalyst, indicating very low steady-state surface concentrations of adsorbed N_2O. These DRIFTS results are consistent with the following catalytic redox mechanism proposed for N_2O decomposition over Cu–ZSM-5. Gas-phase N_2O adsorbs molecularly via the O end onto a Cu^+ ion at a $Si–O^-Cu^+$ site maintained in a highly dispersed state. This adsorbed N_2O species then irreversibly decomposes in a rate-determining step to form gaseous N_2 and an adsorbed O atom. In the process Cu^+ is oxidized to Cu^{2+}, which is stabilized as either $Si–O^-[Cu^{2+}(O^-)]^+$ or $Si–O^-[Cu^{2+}(OH^-)]^+$. When two such sites are located in close proximity, such as at opposite corners of a four-membered ring having Al tetrahedra at the T9 sites of ZSM-5, oxygen recombination can readily occur to form O_2, and in the process Cu^{2+} is reduced to Cu^+, thus completing the redox cycle. This mechanism incorporates aspects specific to both the copper ions and the zeolite structure to explain the uniquely high activity of this particular catalyst, and the rate expression derived from this model fits the data well over a wide temperature range.

INTRODUCTION

Nitrous oxide (N_2O) decomposition has been studied primarily as a test reaction to evaluate the catalytic activities of oxides and to probe the properties of solids (1, 2). It also has been used to determine metal surface areas of supported catalysts (3). Similar to the NO_x gases (NO and NO_2), N_2O is thermodynamically unstable below 1000 K at atmospheric pressure, and calculations assuming ideal gas behavior predict essentially complete decomposition to N_2 and O_2 for this exothermic reaction ($\Delta H_r = -82 \pm 1$ kJ/mol N_2O between 300 and 1000 K) (4). Despite its favorable decomposition thermodynamics, N_2O is quite stable kinetically in the absence of suitable catalysts, but it is effectively decomposed to N_2 and O_2 over numerous zeolite catalysts exhibiting a wide range of activities (5, 6). These data indicate that both a metal and a suitable support are required to produce the most active nonprecious-metal-containing catalyst, namely, Cu-exchanged ZSM-5. The parent material, Na–ZSM-5, is inactive under similar conditions.

Cu–ZSM-5 is active not only for N_2O decomposition but also for NO decomposition and reduction (7–9). For this reason, considerable effort has been directed at characterizing this catalyst to try to elucidate the NO decomposition mechanism (10–28); however, less emphasis has been placed on studying N_2O decomposition although interest in this reaction is being spurred by the recognition of N_2O as a major stratospheric source of NO (29) and as a greenhouse gas (30). A review of the heterogeneous catalytic decomposition of N_2O has recently been published (31), as have investigations using ion-exchanged ZSM-5 (32–40), ZrO_2 (41), Cu–ZrO_2 (42), CuO/γ-Al_2O_3 (43), and Rh supported on zirconia-based catalysts (44, 45).

N_2O decomposition generates reaction products (N_2 and O_2) that are typically IR-inactive. Thus the decomposition behavior of N_2O could, in principle, be readily monitored without the interference of bands from gas-phase products if IR-active surface species exist; however, infrared investigations involving N_2O decomposition have been limited. Room-temperature IR adsorption studies have been conducted using ZnO (46), η-Al_2O_3 (47), α-Cr_2O_3 (48), and ion-containing A and Y zeolites (49, 50), while α-Fe_2O_3

[1] Current address: Union Carbide Corporation, a subsidiary of the Dow Chemical Company, P.O. Box 50, Hahnville, LA 70057.

[2] To whom correspondence should be addressed. Fax: (814) 865-7846. E-mail: mavche@engr.psu.edu.

0021-9517/02 $35.00

has been studied at elevated temperatures (51). Fe–Y has been studied by IR spectroscopy, but not directly in conjunction with N_2O decomposition (52). Photocatalytic decomposition of N_2O has been studied on highly dispersed Ag/TiO_2 (53), and UV diffuse reflectance spectra were obtained with a Cu–ZSM-5 catalyst used for photocatalytic N_2O decomposition below room temperature (54, 55). Diffuse reflectance infrared Fourier transform spectroscopy (DRIFTS) has been used to examine dehydrated and dehydroxylated H–ZSM-5 at 300 K (56–58) and to obtain spectra of CO adsorbed on Cu–ZSM-5 catalysts (33, 40), but no N_2O-related spectra have been reported. The dynamics of N_2O decomposition on an overexchanged Cu–ZSM-5 catalyst have been studied under transient oxidizing and reducing conditions, but no inhibiting effect of O_2 was reported for this catalyst (32), which is contrary to other studies with Cu–ZSM-5 (5, 31, 33, 40).

Because no detailed Fourier transform infrared (FTIR) studies of N_2O decomposition using nominally overexchanged Cu–ZSM-5 had been reported, an *in situ* investigation of this powdered catalyst was undertaken with the intent of monitoring the entire process by DRIFTS, including catalyst pretreatment, transient changes during N_2O introduction, and steady-state N_2O decomposition, to learn as much as possible about the state of the zeolite catalysts as well as the presence of any surface species. This behavior was compared with that of Na–ZSM-5 in an attempt to clarify the roles of the metal and the zeolite in this reaction on these very active Cu–ZSM-5 catalysts.

EXPERIMENTAL

All ZSM-5 catalysts were provided by Air Products and Chemicals, Inc., and were synthesized using template-free protocols. Zeolite catalyst designations and pertinent compositional information are contained in Table 1. The Cu–ZSM-5a catalyst was prepared via ion exchange of the listed parent Na–ZSM-5 (5, 6, 59). A different, commercial zeolite in the NH_4^+ form served as the basis for the Cu–ZSM-5n catalyst (60). After ion exchange from aqueous solution, each catalyst was filtered, thoroughly washed, and air dried at 383 K overnight. Neither the Na–ZSM-5 nor the Cu–ZSM-5 samples were calcined prior to DRIFTS analysis. No spectral evidence was obtained to indicate that the difference in the Si/Al ratio between the two Cu–ZSM-5 catalysts had any significant effect on catalyst behavior (61).

Only minor modifications to an existing gas-handling system (62) were necessary in order to conduct the DRIFTS studies. A molecular sieve trap containing 5A zeolite (Davison Chemical, Grade 522) was added to the line supplying Ar (Liquid Carbonic, 99.999%), and a cylinder containing 0.509% N_2O/Ar (Matheson, <71 ppm total impurities) was attached. Other gases used included ultrahigh-purity-grade N_2 (MG Industries, 99.999%), N_2O (Matheson, 99.99%), O_2 (MG Industries, 99.999%), and CO (Matheson, 99.99%). The N_2 and N_2O as well as the N_2O gas mixture were used without further purification.

Approximately 45 mg of Na–ZSM-5 or 35 mg of Cu–ZSM-5 was loaded into the microsampling cup of the 2-D car or into the top of the post in the HVC-DRP reactor. All additional connection, purge, and height-adjustment protocols were the same as for the gas-phase procedures (61). The standard pretreatment consisted of heating in Ar (typically 20 sccm) from 300 to 773 K at 5 K/min and holding at 773 K for 1 h. After pretreatment, each catalyst sample was cooled in Ar to the appropriate temperature for background data collection, i.e., 300, 583, 603, 623, 643, or 673 K, as noted in the figure captions, prior to exposure to N_2O (0.1 or 0.5%), N_2 (2 or 4%), O_2 (10%), or CO (1%). Interferograms were obtained during the gas introduction as well as under steady flow or steady-state decomposition conditions, and spectra for the latter were typically initiated after at least 20 min of flow. For multiple temperature experiments, each subsequent steady-state interferogram was usually obtained 15 min after first reaching the next desired temperature. Purging of gases was also monitored and these scans were begun after at least 20 min of purging in Ar.

Data acquisition consisted of using an upgraded Sirius 100 FTIR (Mattson Instruments, Inc.) equipped with a liquid nitrogen-cooled MCT detector to collect interferogram data of either 100 (transient) or 1000 (steady-state) signal-averaged scans at 4 cm^{-1} resolution, which required a minimum of ~1 or ~8 min, respectively. Appropriate sample and background interferograms were individually Fourier transformed using triangular apodization to yield the corresponding frequency-component sample and

TABLE 1

Catalyst Designations and Pertinent Compositional Information

Catalyst designation	Exchange material	Si (wt%)	Al (wt%)	Cu (wt%)	Na (wt%)	LOI[a] (wt%)	Si/Al	M/Al[b]
Na–ZSM-5	—	42.2	2.96	—	2.56	10.55	13.8	1.01
Cu–ZSM-5a	$Cu(CH_3COO)_2$	36.3	2.60	3.69	0.04	11.00	13.5	0.60
Cu–ZSM-5n	$Cu(NO_3)_2$	39.6	3.55	4.56	<0.02	8.51	10.7	0.55

[a] LOI, loss on ignition.
[b] M = Cu or Na.

background single-beam spectra, the ratio of which gave a reflectance (R) spectrum from which either an "absorbance" spectrum [$A = \log(1/R)$] or a Kubelka–Munk spectrum [$\text{K–M} = (1-R)^2/2R$] was ultimately obtained. A sample interferogram for one spectrum could also serve as the background interferogram for another to create difference spectra. Absorbance spectra using either open-beam or Al-mirror backgrounds were routinely similar to the corresponding K–M spectra, as were spectra exhibiting only positive absorbance features; however, because negative bands in a difference spectrum will be inverted in the corresponding K–M spectrum due to its functional form, only "absorbance" spectra are shown here. Gas-phase N_2O spectra were obtained after an overnight purge with Ar by flowing an appropriate concentration of N_2O in Ar through the HVC-DRP reactor cell, which contained an aluminum mirror specially designed to fit in the sample area at the top of the post. Additional details regarding the experimental apparatus and procedures are available (61–64).

RESULTS

Spectra of the as-charged ZSM-5 samples at 300 K are shown in Fig. 1, with the open-beam condition as background. Figures 1b and 1c represent spectra of two different samples of Cu–ZSM-5a. In addition to zeolite-related bands near 1965, 1865, 1630, 1195, 1080–1040, and 800 cm^{-1} (65–74), absorbance features are observed in three predominant regions, namely, 3800–2500, 1400–1300, and 1000–900 cm^{-1}. The broad band between 3800 and 2500 cm^{-1} is indicative of hydrogen-bonded O–H stretching contributions from molecularly adsorbed and/or coordinated H_2O, as well as from surface Si–OH groups and other species in heterogeneous environments introduced during or resulting from the ion-exchange process, such as silanol nests and vicinal silanol groups (74–78). The breadth of this absorbance frequently obscures any well-defined peaks; however, resolved peaks near 3335, 3275, and 3185 cm^{-1} with Cu–ZSM-5n indicate the presence of O–H and N–H stretching modes (67, 76, 79), the latter apparently due to its NH_4^+ precursor form. A band at 3360 cm^{-1} has been assigned to NH_3 adsorbed on copper in a 523%-exchanged Cu–ZSM-5 sample (32). After exposure of Fe–ZSM-5 to NH_3, bands at 3353 and 3290 cm^{-1} were assigned to NH_4^+ ions with three H atoms bonded to three O ions in AlO_4 tetrahedra, whereas bands at 3050 and 2795 cm^{-1} were assigned to NH_4^+ ions with two H atoms bonded to AlO_4 tetrahedra (78). Just barely discernible is the crystal terminating or extra-zeolitic Si–OH band near 3735 cm^{-1} (28, 67, 73–82), and some contribution to the 3666-cm^{-1} feature for Na–ZSM-5 is likely due to Al–OH absorbances (28, 65, 74–77, 82). The bands at 2923 and 1670 cm^{-1} can be attributed to residual acetate in the sample.

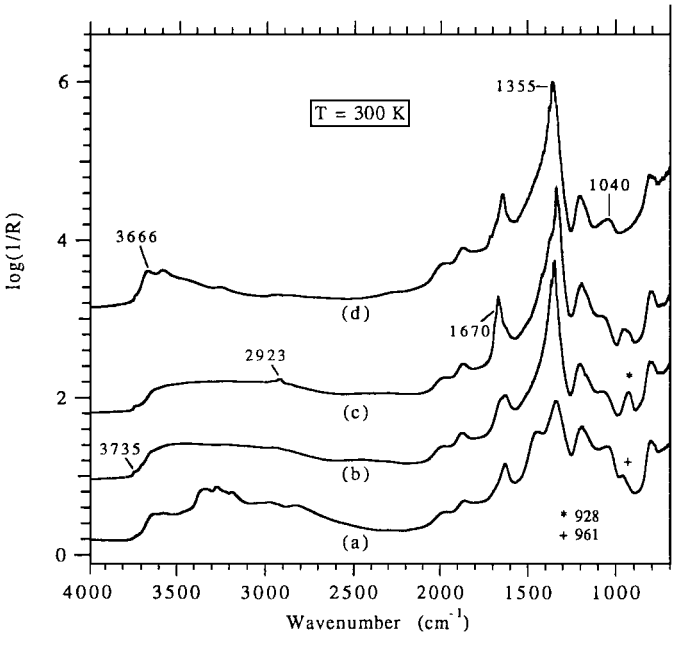

FIG. 1. Spectra of the as-charged ZSM-5 samples at 300 K: (a) Cu–ZSM-5n; (b) Cu–ZSM-5a (Sample 1); (c) Cu–ZSM-5a (Sample 2); and (d) Na–ZSM-5. The background for each spectrum is the open-beam condition.

In contrast to Na–ZSM-5, for which no band was observed between 1000 and 900 cm^{-1} (73, 83), each ion-exchanged zeolite exhibited an absorbance feature in this range which has been associated with $Si–O^-$ stretching vibrations and highly strained or broken siloxane bridge surface defects (84–92), due in part to the presence of extralattice oxygen (ELO) incorporated during the catalyst preparation (73). An assignment has also been made to an internal asymmetric framework vibration perturbed by copper cations (74, 83). As summarized in Table 2, the position of this peak may depend on the exchange anion and precursor form of the zeolite, and its width may be influenced by the presence of residual hydrated acetate (93–98). The peak *maximum* fell between 961 and 926 cm^{-1} with the Cu–ZSM-5 samples and varied only between 959 and 953 cm^{-1} with Co–ZSM-5a (61).

Even though it is the most intense feature in the ZSM-5 spectra, the asymmetric absorbance peak between 1400 and 1300 cm^1 provides no information because it is associated with strong lattice vibrations that produce a specular reflectance contribution to the signal. This problem is especially severe in DRIFT spectra of neat samples because this band disappeared when Cu–ZSM-5a was diluted with KBr, and no such peak was observed when undiluted Cu–ZSM-5a was examined by *transmission* IR through a pressed wafer (61). A similar absorbance feature of comparable intensity and shape was observed for other undiluted oxides of various particle sizes, with peak positions at 1365 cm^{-1} for SiO_2, 1050 cm^{-1} for η-Al_2O_3, and 930 cm^{-1} for TiO_2 (61).

TABLE 2

Peak Positions and Assignments for ZSM-5 Samples

Figure	Catalyst	Peack Center (cm^{-1})[a]											
		A	B	C	D	E	F	G	H	I	J	K	L
1a	Cu–ZSM-5n	3725	—	1960	1860	—	1629	1445	1335	1190	1043	960	803
1b	Cu–ZSM-5a	3735	—	1970	1873	1660[b]	1628	—	1350	1200	1070	930	800
1c	Cu–ZSM-5a	3735	2923[c]	1965	1868	1670	1630[b]	1417[b]	1335	1192	1080	940[d]	800
1d	Na–ZSM-5	3740	—	1965	1865	—	1635	—	1355	1197	1040	—	800

[a] A, υO–H stretching virbration of terminal or extrazeolitic Si–OH. B, C–H stretching vibration of acetate (OAc) ion. C, Combination band of T–O fundamental lattice ring vibration (T = Si, Al). D, Combination band of T–O fundamental lattice ring vibration. E, C=O stretching vibration of acetate (OAc) ion. F, Combination/overtone band of T–O fundamental lattice ring vibration; deformation vibrations of molecularly adsorbed water; υ_2 fundamental of physisorbed water (H–O–H bending). G, Possibly δ_{N-H} for Fig. 1a. H, An artifact attributed to specular reflectance. I, External υ_{as} (T–O–T). J, Internal υ_{as} <–OT–><–O (internal vibrations of framework TO_4 tetrahedra). K, υSi–O$^-$; band related to extralattice oxygen; internal υ_{as} perturbed by copper cations (Cu^+ and Cu^{2+}). L, υ_s of <–OTO–> linkages.

[b] Appears as a shoulder.

[c] Present when either open beam or Al mirror used as background.

[d] Maximum at 950 cm^{-1}.

Pretreatment of Na–ZSM-5 resulted in the removal of water, and from the broad absorbance in the O–H stretching region in Fig. 1 emerged two small bands of roughly equal intensity, near 3734 and 3666 cm^{-1}, for crystal-terminating or isolated Si–OH and extra-zeolitic Al–OH functionalities (28, 65, 67, 73–82), respectively. The band originally centered at 1040 cm^{-1} redshifted to near 1020 cm^{-1}. No detectable peaks were observed in the 2200- to 2000-cm^{-1} region.

As seen in Fig. 2, contacting Na–ZSM-5 with 0.1% N_2O caused noticeable spectral changes in the O–H stretching region, and the time-evolved spectra clearly show the development of a band centered near 3585 cm^{-1} that had a small shoulder at 3685 cm^{-1}, most likely for Al–OH (28, 65, 74–77, 82). Increasing the temperature attenuated these bands. The band near 1645 cm^{-1} is attributed to the bending mode of H_2O (65, 66, 87, 99, 100), but some enhancement of the zeolite-related combination band cannot be excluded (65–67, 99). Minor intensity enhancement was noticed at steady state in the 910- to 845-cm^{-1} region at 583 K (61). No adsorbed species were detected in the presence of gas-phase N_2O after subtracting the gas-phase spectrum for 0.1% N_2O that gave the bands near 2236 and 2211 cm^{-1}, which were in good agreement with published results (101–104).

Heating acetate-exchanged Cu–ZSM-5a in Ar caused noticeable spectral changes in three regions, namely 3800–2500, 1000–900, and 2200–2100 cm^{-1}, while zeolite-related bands exhibited minor variations. Intensity decreases in Fig. 3 between 3800 and 2500 cm^{-1} as well as near 1630 cm^{-1} indicate that water began to desorb prior to 388 K, very near the temperature at which temperature-programmed desorption (TPD) experiments have found a maximum for H_2O (61). Above 408 K, other O–H bands could be seen, particularly that near 3600 cm^{-1}, which is attributed to the O–H stretching vibration of acidic Si(OH)Al bridging hydroxyl groups (28, 67, 74–77, 79, 80). A band at 3731 cm^{-1} for isolated terminal or extra-zeolitic Si–OH was better resolved (28, 67, 73–80), and at 478 K a shoulder feature can be seen at 3667 cm^{-1}, which is assigned to the O–H stretching vibration of Al–OH (28, 65, 74–77, 82) or $[Cu^{2+}(OH^-)]^+$

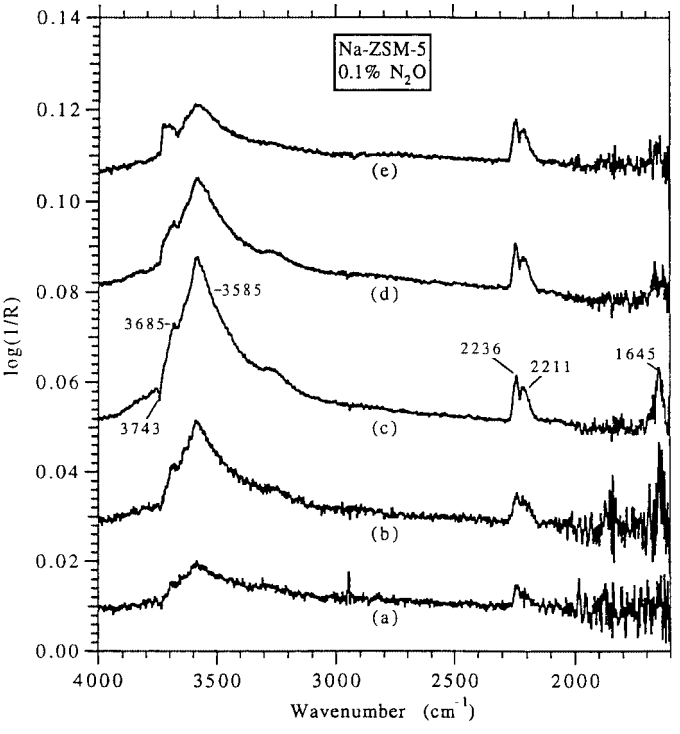

FIG. 2. Exposure of Na–ZSM-5 to 0.1% N_2O. Time of initiating data acquisition relative to beginning to flow N_2O at 583 K: (a) 1.13, (b) 3.42, and (c) 15.0 min. Steady-state N_2O flow at (d) 603 and (e) 643 K. The background is the state of the catalyst just before exposure to N_2O at the respective temperature.

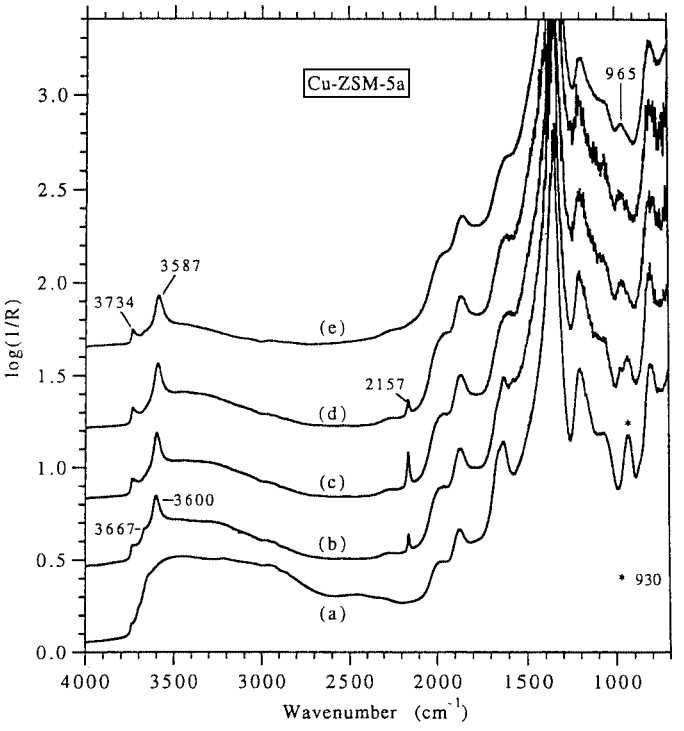

FIG. 3. Spectra of Cu–ZSM-5a during pretreatment. Data acquisition was begun at the following temperatures: (a) 314, (b) 478, (c) 583, (d) 668, and (e) 773 K. The background for each spectrum is the open-beam condition.

groups (73). Even after 1 h at 773 K, considerable amounts of hydrogen-bonded O–H groups were present, as evidenced by the ubiquitous broad band between 3800 and 2800 cm^{-1} (74–77). The terminal Si–OH peak near 3734 cm^{-1} remained essentially unaffected by the pretreatment whereas the bridging Si(OH)Al band at 3600 cm^{-1} at 478 K continuously decreased to 3587 cm^{-1} at 773 K. As the 930 cm^{-1} band intensity decreased, a band near 965 cm^{-1} simultaneously appeared and increased as temperature increased. A very small, yet distinct, band at 2157 cm^{-1} was readily observed at 478 K and passed through a maximum intensity near 583 K, similar to the CO_2 and CO mass spectrometer signals exhibited during TPD experiments (61). This feature is assigned to CO adsorbed on cuprous ions (8, 9, 28, 32, 33, 74, 75, 105–108). Similar to CO_2, the CO was most likely produced from the thermal decomposition of residual acetate, while the Cu^+ was evidently formed by autoreduction of Cu^{2+} during heating. This latter conclusion is supported by electron spin resonance (ESR) spectra showing a 96% reduction of the Cu^{2+} signal strength after pretreatment, with diamagnetic Cu^+ being the most probable reduction product (54, 61, 77, 109–112). Little or no carbon was present because its ESR features remained absent after dehydration at 773 K, a state where only a small fraction of the original Cu^{2+} intensity remained. Indeed, no trace of the 2157-cm^{-1} band was detected after 0.5 h at 773 K; thus these data suggest that the thermal reduction of Cu^{2+} in Cu–ZSM-5a readily occurs during this pretreatment.

Although the chemistry seemed to be different due to its NH_4^+ precursor form, pretreatment of Cu–ZSM-5n induced changes in essentially the same regions as for Cu–ZSM-5a. As shown in Fig. 4, these changes included the loss of H_2O above 383 K and the concomitant delineation of peaks for bridging Si(OH)Al groups and isolated terminal or extra-zeolitic Si–OH structures. Hydrogen-bonded O–H groups were also present at 773 K. Unlike the copious changes in the υO–H region, minimal changes were observed in the 1000- to 900-cm^{-1} range, with the small band originally at 961 cm^{-1} gradually shifting to a 970-cm^{-1} shoulder at 773 K. There was no evidence for a band at 2157 cm^{-1}. All in all, the spectrum for Cu–ZSM-5n after heating to 773 K was nearly identical to that for Cu–ZSM-5a (Fig. 3e).

After the introduction of N_2O at 583 K, FTIR spectral features not seen with Na–ZSM-5 were quickly detected with Cu–ZSM-5a (Fig. 5) and Cu–ZSM-5n (Fig. 6). With the former, a faint decrease near 3739 cm^{-1} was accompanied by a more substantial decrease near 3597 cm^{-1}, as shown in Fig. 5, indicating the destruction of isolated terminal Si–OH and bridging Si(OH)Al groups, respectively. Concurrent with these losses was the apparent growth of

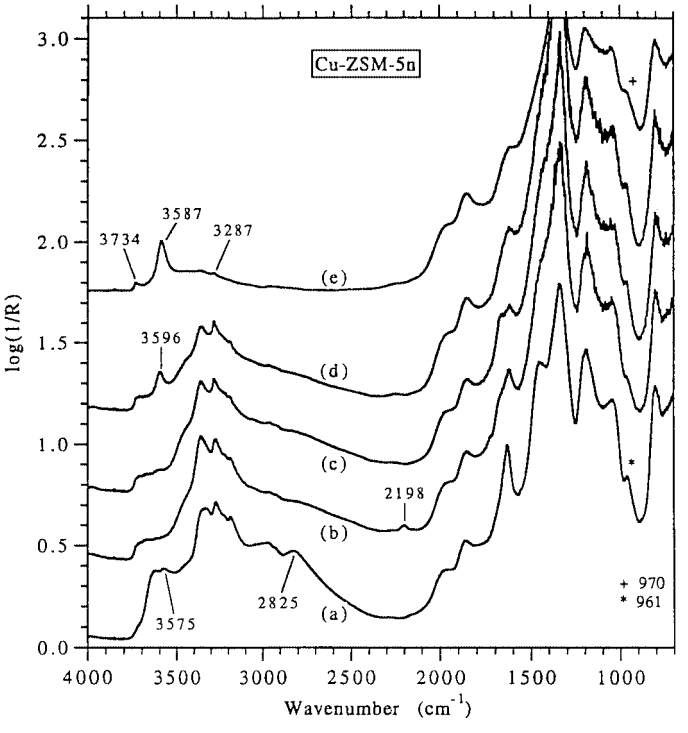

FIG. 4. Spectra of Cu–ZSM-5n during pretreatment. Data acquisition was begun at the following temperatures: (a) 313, (b) 473, (c) 548, (d) 648, and (e) 773 K. The background for each spectrum is the open-beam condition.

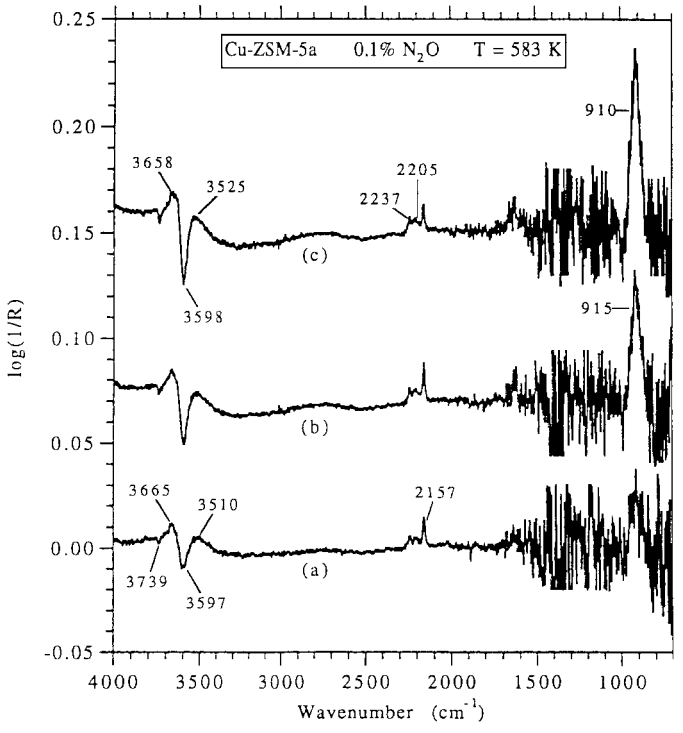

FIG. 5. Exposure of Cu–ZSM-5a to 0.1% N_2O at 583 K. Time of initiating data acquisition relative to beginning to flow N_2O: (a) 1.12, (b) 3.70, and (c) 5.87 min. The background is the state of the catalyst just before exposure to N_2O.

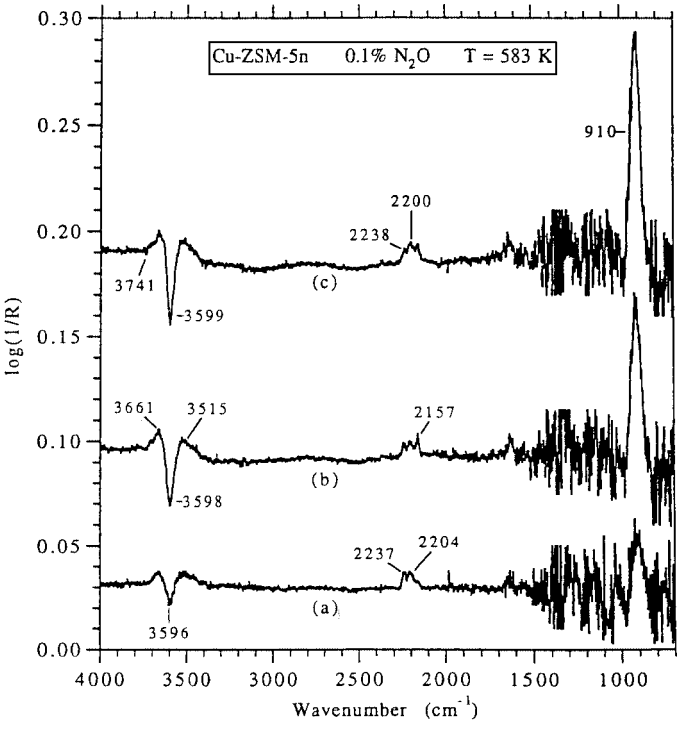

FIG. 6. Exposure of Cu–ZSM-5n to 0.1% N_2O at 583 K. Time of initiating data acquisition relative to beginning to flow N_2O: (a) 1.08, (b) 3.30, and (c) 5.50 min. The background is the state of the catalyst just before exposure to N_2O.

a broad band throughout this region. Similar behavior has been observed for methane adsorption at 173 K on outgassed H–ZSM-5 (113). Weak bands for gas-phase N_2O were observed along with a band near 2157 cm^{-1}, which was likely due to N_2 adsorbed on coordinatively unsaturated Cu^+ sites (25, 32, 114–116). As opposed to Cu^+–CO, an assignment to Cu^+–N_2 is favored not only because N_2 was quickly detected by mass spectroscopy during a separate exposure of this catalyst to N_2O at 603 K, but also because this band occurred when N_2 was flowed at 300 K over either a purged sample of N_2O-exposed Cu–ZSM-5a or a sample that had been freshly re-pretreated (61). In the latter case, a band initially appeared at 2296 cm^{-1}, which is consistent with a band at 2295 cm^{-1} observed by Zecchina and coworkers (117, 118); however, with Cu–ZSM-5a this peak converted completely to the 2157 peak (61). This peak near 2157 cm^{-1} passed through an absorbance maximum for each catalyst and then decreased as exposure time increased. Concurrent with the presence of this sharp band and the changes in the O–H stretching region, absorbance increased in the $\upsilon Si–O^-$ region and eventually became a symmetric peak centered around 915–910 cm^{-1}, which signifies the interaction of adsorbed O atoms (i.e., extralattice oxygen) with the catalyst and can be associated with Cu^{2+} species, as shown by Zecchina and coworkers (112). Despite the poor signal-to-noise ratio, absorbance enhancement can be detected near ~1630 cm^{-1}, where an assignment to bridging $[Cu^{2+}(NO_3^-)]^+$ has been made (32), but it could also represent the bending mode of H_2O or an enhancement of a zeolite-related combination band.

Other than the 2157-cm^{-1} peak, no obvious spectral evidence existed for any adsorbed species; however, a difference spectrum at 583 K for Cu–ZSM-5 revealed the presence of an adsorbed species whose small band lay under the gas-phase envelope for N_2O, as shown in Fig. 7a for Cu–ZSM-5n. Because this absorbance was overlapped by the gas-phase N_2O bands, it likely signified a surface N_2O species, such as Cu^+–ON_2 (32). A transient band was observed at 300 K near 2294 cm^{-1}, in the region where previous assignments to Cu–N_2 (117–120) and N_2O adsorbed on Cu^+ via the end N atom (Cu^+–N_2O) (32) have been made, but the latter band was not detected during the introduction of 0.1% N_2O at 583 K for either Cu–ZSM-5a or Cu–ZSM-5n.

When the spectra in Fig. 5 are compared to that in Fig. 8a, limited changes can be observed between the transient and steady-state reaction periods at 583 K for Cu–ZSM-5a. In contrast, the Cu–ZSM-5n in Fig. 9 showed modifications in zeolite-related bands near 1960, 1870, and 1630 cm^{-1}, and an increase near 1360 cm^{-1} had the same characteristics as the band in Fig. 1 ascribed to a DRIFTS-related artifact. Changes that occurred for Cu–ZSM-5a during the 20-min period from the end of the last $n = 100$ transient interferogram to the end of the $n = 1000$ steady-state interferogram

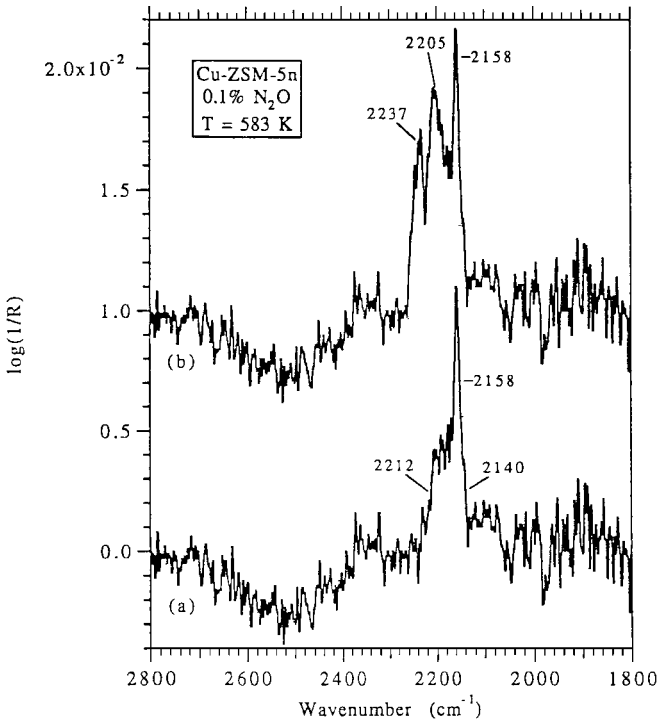

FIG. 7. Adsorbed species on Cu–ZSM-5n during the introduction of 0.1% N_2O at 583 K. Spectrum (a) was created by computer-subtracting the gas-phase N_2O contribution from (b). The background is the state of the catalyst just before exposure to N_2O exposure.

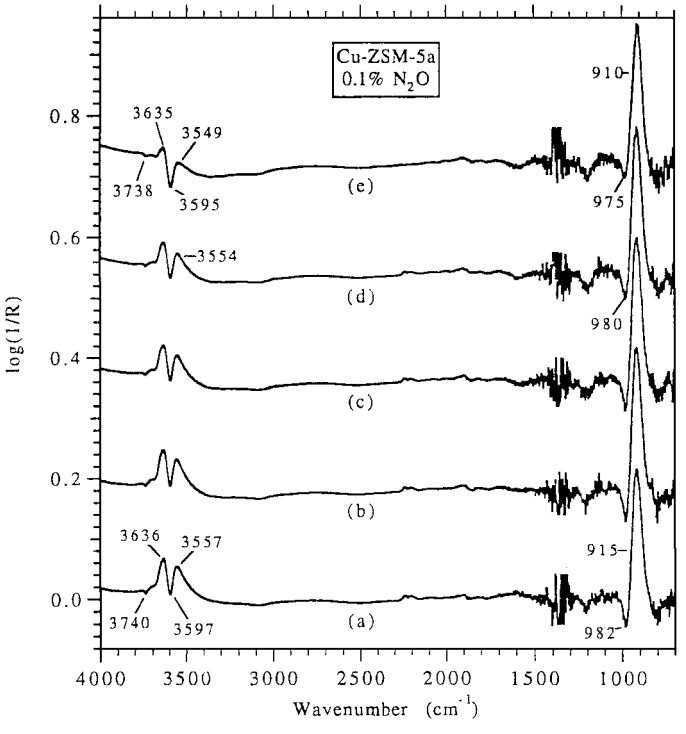

FIG. 8. Steady-state N_2O decomposition during exposure of Cu–ZSM-5a to 0.1% N_2O. Temperatures: (a) 583, (b) 603, (c) 623, and (d) 643 K. Spectrum (e) shows the changes due to exposure and then purging at 643 K. The background for each spectrum is the state of the catalyst at the designated temperature prior to N_2O exposure.

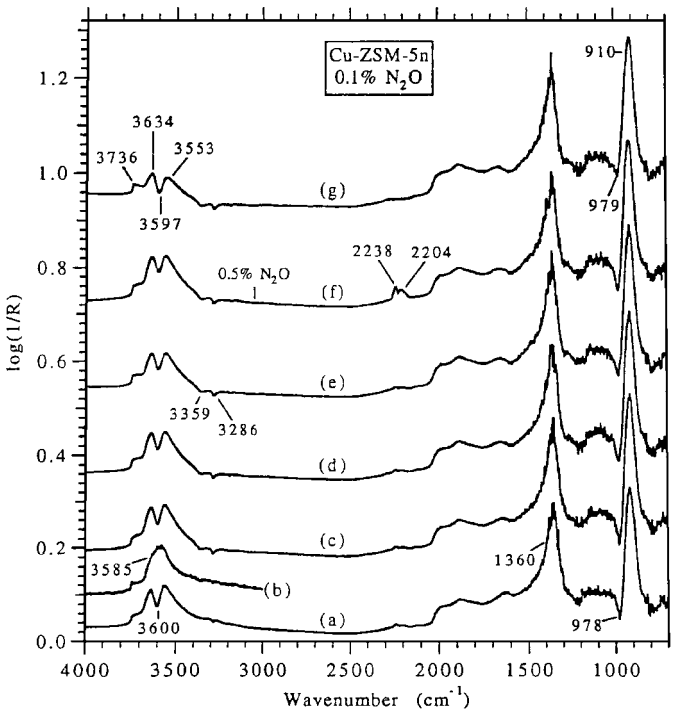

FIG. 9. Steady-state N_2O decomposition during exposure of Cu–ZSM-5n to 0.1% N_2O. Temperatures: (a) 583, (b) 583, (c) 603, (d) 623, (e) 643, (f) 643 (0.5% N_2O), and (g) 643 K. Spectrum (b) was created by subtracting from (a) the spectrum begun 5.50 min after beginning to flow N_2O. Spectrum (g) shows the changes due to exposure and then purging at 643 K. The background for each spectrum is the state of the catalyst at the designated temperature prior to N_2O exposure.

are shown in Fig. 10a. Enhancement of the high-intensity band near 915 cm^{-1} in Fig. 8a is apparent in Fig. 10a, and elimination of the 2157-cm^{-1} band was also effected during this time, while intensity enhancement between 3700 and 3400 cm^{-1} also occurred.

At steady-state N_2O decomposition conditions, the Cu–ZSM-5a and Cu–ZSM-5n catalysts show no major IR-detectable changes from 583 to 643 K, and the spectra in Fig. 8 and Fig. 9 change little. However, as seen in Fig. 10b, an Ar purge at 643 K caused a decrease centered at 928 cm^{-1} as well as decreases for bands in the O–H stretching region, with the largest decrease at 3571 cm^{-1} accompanied by discernible losses at 3610 and 3642 cm^{-1}. Similar results were obtained with Cu–ZSM-5n (61). No unequivocal evidence for any adsorbed N_2O species was found during steady-state decomposition on either Cu–ZSM-5a or Cu–ZSM-5n, and of all the changes observed for these two catalysts, the most intense absorbance increase was that in the υSi–O^- region near 915 cm^{-1}. This is apparent in the difference spectra (Fig. 10a) as well as the spectra in Fig. 11. The major change was the shift of the 966 cm^{-1} band to 920 cm^{-1}, whereas only very small fractions of the isolated terminal Si–OH, briding Si(OH)Al, and H-bonded O–H groups were affected by the decomposition reaction.

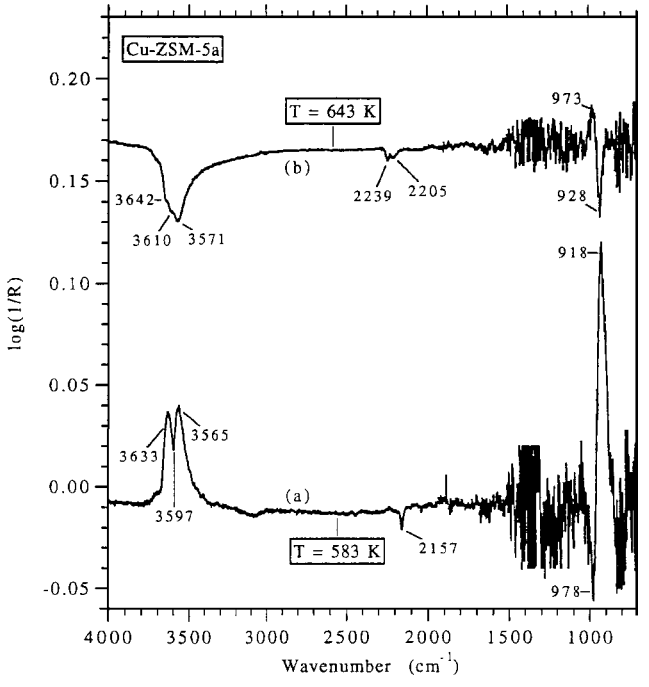

FIG. 10. Difference spectra more clearly showing the changes between the selected sample and background states during exposure of Cu–ZSM-5a to 0.1% N_2O. Sample with respect to background: (a) N_2O decomposition at 583 K with respect to unsteady condition during min 8 of flow at 583 K; and (b) purged catalyst at 643 K with respect to the catalyst prior to purge.

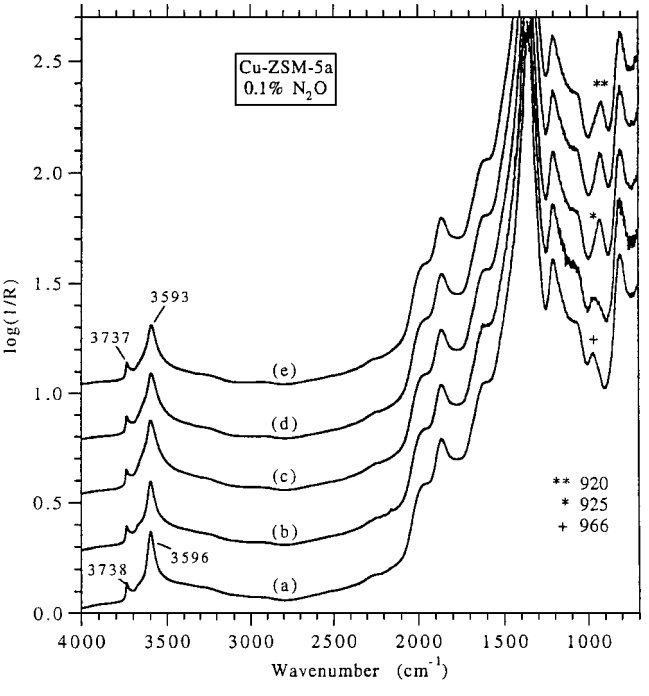

FIG. 11. Spectra showing global changes due to exposure of Cu–ZSM-5a to 0.1% N_2O. Sample interferograms: (a) after pretreatment and just before N_2O at 583 K; (b) during min 7 of flow at 583 K; (c) during steady-state decomposition at 583 K; (d) during steady-state decomposition at 643 K; and (e) after purging N_2O with Ar at 643 K. The background for each spectrum is the Al mirror in the DRIFTS reactor.

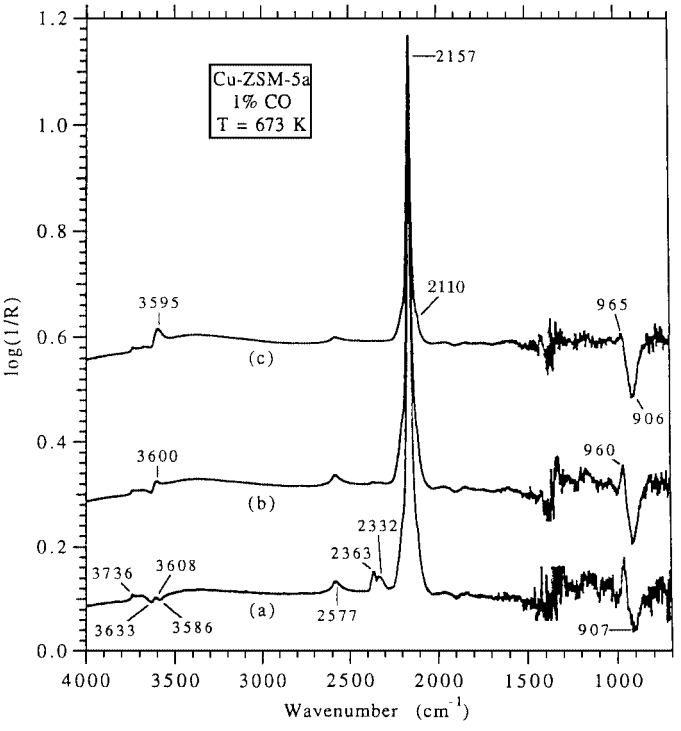

FIG. 12. Changes resulting from exposure of Cu–ZSM-5a to 1% CO at 673 K after having been subjected to various experimental procedures. Spectra: (a) during min 2 of CO flow; (b) after 48 min in CO; and (c) after purging CO at 673 K. The background is the state of the catalyst just before exposure to CO.

In one experiment, after pretreating Cu–ZSM-5a at 773 K and cooling to 603 K, the catalyst was exposed to 10% O_2 instead of 0.1% N_2O. After 2 min the resulting spectrum was essentially identical to that in Fig. 8b, and further O_2 exposure caused little change even though the O_2 concentration was orders of magnitude higher than that during the N_2O decomposition experiments. A sample of Cu–ZSM-5a was heated to 673 K and exposed to 1% CO, which markedly enhanced the IR band initially present at 2157 cm^{-1}, as shown in Fig. 12. This band is assigned to a CO molecule adsorbed on a cuprous ion (Cu^+–CO) (8, 9, 28, 32, 33, 74, 75, 105–108, 118), and its intensity is consistent with a highly dispersed state for the Cu^+ ions. A significant amount of gas-phase CO_2 (bands at 2363 and 2332 cm^{-1}) was concurrently detected along with an absorbance increase near 960 cm^{-1} and a decrease near 907 cm^{-1}. Changes in the υO–H region demonstrated that the CO affected the Brønsted acidic bridging Si(OH)Al groups near 3600–3595 cm^{-1}, and a new feature near 2577 cm^{-1} appeared. The spectrum in Fig. 12a, acquired within 2 min after introduction of CO, captures the major IR-observable changes that resulted. Essentially all of the gas-phase CO_2 disappeared within 2 min of first being detected. After a 48-min exposure to CO, the peak near 3600 cm^{-1} and the loss peak at 906 cm^{-1} became better defined, then purging at 673 K reduced the

2157-cm^{-1} band intensity by 33%. Spectra referenced to Al-mirror backgrounds showed that exposure to CO produced a well-defined peak centered near 961 cm^{-1}, and the shape of this band and the overall spectrum were very similar to those in Figs. 3d and 3e, except for a more intense 2157-cm^{-1} band (61). Comparison of the spectra in Fig. 12 to those in Figs. 5 and 6 shows that exposure of Cu–ZSM-5 to CO (a reductant) caused spectral changes in the υO–H and υSi–O$^-$ regions that were opposite to those after exposure to N_2O (an oxidant).

DISCUSSION

Ion-Exchange and Pretreatment Steps

After a purge in Ar at 300 K, the Cu–ZSM-5 catalysts exhibited a broad absorbance in the O–H stretching region (3800–2500 cm^{-1}) as well as a band in the δO–H region near 1630 cm^{-1}, indicative of H-bonding interactions involving coordinated water (77). ESR and related electron spin–echo modulation results suggest that all of the copper ions are originally present in a hydrated octahedral $Cu^{2+}(H_2O)_6$ configuration (121). Because these bulky complexes (7.4 Å for Cu^{2+}) are larger than the nominal 5- to 6-Å pore openings of ZSM-5 (121), they are believed to be located at the 10-membered-ring channel intersections, which form cavities approximately 9 Å in diameter (27). Temperature-dependent ESR spectra for the as-received Cu–ZSM-5a indicated mobile species (61), further supporting the location of the hydrated Cu^{2+} ions at the channel intersections.

During pretreatment, a band near 3600 cm^{-1} assigned to Si(OH)Al bridging hydroxyl groups was detected for the Cu–ZSM-5 catalysts. At least part of this Brønsted acidity is created during ion exchange (73, 122) by hydrolysis of octahedral $Cu^{2+}(H_2O)_n$ complexes (123), i.e.,

$$Cu^{2+}(H_2O)_n \rightleftharpoons [Cu^{2+}(H_2O)_{n-1}(OH^-)]^+ + H^+ \quad (n = 6). \qquad [1]$$

The interaction of water with the strong electrostatic field of the Cu^{2+} cations results in the generation of Brønsted acid centers (124), and additional protons can be liberated during heating as H_2O ligands are removed. Because the $[Cu^{2+}(H_2O)_{n-1}(OH^-)]^+$ complex differs from $Cu^{2+}(H_2O)_n$ by only one proton, it still must be quite large and should also be located at the channel intersections, which is also where the Si(OH)Al groups are believed to exist (125, 126). The presence of the latter groups signifies that at least a part of the framework charge is now being balanced by protons. Both $Cu^{2+}(H_2O)_n$ and $[Cu^{2+}(H_2O)_{n-1}(OH^{-1})]^+$ can account for the hydrated state of the as-received samples (109).

The decrease in the broad υO–H spectral region (3800–2500 cm^{-1}) is consistent with the removal of coordinately adsorbed water during pretreatment, represented for Cu as follows (123, 124):

$$Cu^{2+}(H_2O)_n \rightleftharpoons Cu^{2+}(H_2O)_{n-1} + H_2O \qquad [2]$$

and

$$[Cu^{2+}(H_2O)_{n-1}(OH^-)]^+ \rightleftharpoons [Cu^{2+}(OH^-)]^+ + (n-1)H_2O. \qquad [3]$$

A small band near 3665 cm^{-1} assigned to $[Cu^{2+}(OH^-)]^+$ was first detected at 458 K but disappeared at 573 K during pretreatment of Cu–ZSM-5a. Larsen *et al.* assumed that copper was exchanged into Na–ZSM-5 as $[Cu^{2+}(OH^-)]^+$, perhaps because their analyses were performed on samples that had been dried at 373 K (109), and the remainder of the charge compensation was provided by protons (27, 73). Hence, in addition to $Cu^{2+}(H_2O)_n$ and $[Cu^{2+}(H_2O)_{n-1}(OH^-)]^+$, $[Cu^{2+}(OH^-)]^+$ complexes could be present in the ion-exchanged samples, and the latter two groups offer reasonable explanations for the "overexchange" behavior reported for certain zeolites (27, 69, 73, 123, 127). Indeed, $[(Cu^{2+})_x(OH^-)_y]^{(2x-y)+}$ polynuclear complexes have been reported to be responsible for the excess loading of copper ions in mordenite (MOR) (123).

The appearance of a band near 2157 cm^{-1} during the initial heating of Cu–ZSM-5a, which was assigned to Cu^+–CO, suggests that thermal reduction of Cu^{2+} to Cu^+ had occurred, and a strong decrease in the Cu^{2+} ESR signal supported this contention (61). Such autoreduction can be described as follows (109):

$$[Cu^{2+}(OH^-)]^+ \rightleftharpoons Cu^+ + OH, \qquad [4]$$

$$[Cu^{2+}(OH^-)]^+ + OH \rightleftharpoons [Cu^{2+}(O^-)]^+ + H_2O, \qquad [5]$$

$$2[Cu^{2+}(OH^-)]^+ \rightleftharpoons Cu^+ + [Cu^{2+}(O^-)]^+ + H_2O. \qquad [6]$$

The $[Cu^{2+}(O^-)]^+$ species has been hypothesized to form during NO decomposition over Cu–ZSM-5 (25, 28, 32), and it gives no detectable ESR signal (83, 109). This ESR-inactive nature can resolve the apparent conflict between the nearly complete (96%) reduction indicated by the ESR data for Cu–ZSM-5a (61) and the 50% reduction implied by Eq. [6], and it suggests that the conversion of $[Cu^{2+}(O^-)]^+$ to Cu^+ and O_2, shown in Eq. [7] is minimal:

$$2[Cu^{2+}(O^-)]^+ \rightleftharpoons 2Cu^+ + O_2. \qquad [7]$$

This obviates the difficulties associated with explaining the required proximity of the $[Cu^{2+}(O^-)]^+$ species necessary for the formation of O_2.

Cation Stabilization in Cu–ZSM-5

Insights into the catalytic role of the zeolite and the nature of the interactions between the ions and the zeolitic framework can be obtained by comparing changes

in the spectra during pretreatment. One new band (3600–3587 cm^{-1}) was readily perceptible during pretreatment of the Cu–ZSM-5 catalysts (Figs. 3 and 5), and it indicated either the preexistence or the creation of bridging Si(OH)Al groups located at channel intersections resulting from the ion-exchange process, at least in part. This agrees with the proposed formation of H^+ via Eq. [1], and the presence of H^+ signifies that at least a part of the framework charge originally balanced by Na^+ or NH_4^+ is now being balanced by protons. This band first appeared at a lower temperature and with higher intensity for Cu–ZSM-5a than for Cu–ZSM-5n, and one possible explanation for these differences could be the higher thermodynamic affinity for exchange of H_3O^+ (and hence H^+) versus Na^+ whereas H_3O^+ and NH_4^+ exhibit nearly equal exchange affinities (68). The Si(OH)Al structures form so the proton is located in close proximity to the Al tetrahedra which bear the excess negative charge, and hence it seems reasonable that the Cu ions could be positioned accordingly, as depicted schematically in Fig. 13 by Structure I with $G = Cu^+$. Contributions from Na^+ are discounted due to the miniscule quantities of Na detected by elemental analyses, but the DRIFTS spectra clearly revealed detectable quantities of H^+-bearing Si(OH)Al groups. Because copper was introduced as cupric ions, Cu^+ would exist only after reduction, but the remaining complexes could be present under other conditions, with their relative concentrations depending on the extent of hydration and oxidation. In principle, the countercation (G) could be $[Cu^{2+}(O^{2-})Cu^{2+}]^{2+}$, $Cu^{2+}(H_2O)_6$, Cu^{2+}, or other variations (i.e., dimeric divalent species), but it would have to be positioned so that it could balance two negative charges. This same schematic (Fig. 13, Structure I) with $G = Cu^+$ has been used to describe the location of cuprous ions exchanged into a sample of H–ZSM-5 (Si/Al = 90) exposed to CuCl vapor at 573 K so as to introduce only Cu^+ (28).

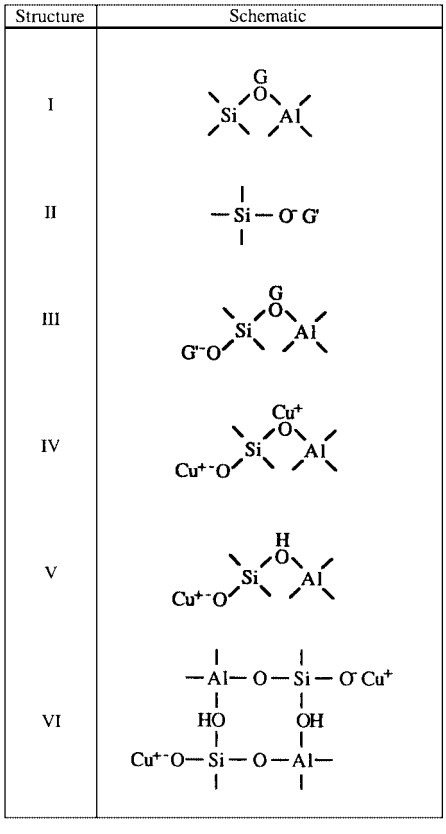

FIG. 13. Schematic representations of sites for stabilized cations in Cu–ZSM-5.

For the Cu–ZSM-5 samples, the new band that develops between 1000 and 900 cm^{-1} is in a region associated with the stretching vibration of Si–O^- bonds (84–91); for example, the room-temperature spectrum of SiO_2 exhibited a band at 977 cm^{-1} (61), and similar assignments have been made for the Si–O^- stretching vibration in Si–OH groups (85, 89, 90, 128), which can be influenced by a cation (i.e., H^+). Consequently, the bands observed in this region for Cu–ZSM-5 are attributed, at least partially, to a comparable configuration, namely, a Cu-perturbed Si–O^- vibration, schematically illustrated as Structure II in Fig. 13. In contrast to Structure I, which maintains the Si–O–Al connectivity, the concentration of species in the form of Structure II must be restricted to minimize deleterious modifications to the framework. The above-noted Si–O^-G' structure is subtly, but nonetheless significantly, different from the Cu-modulated Si–O vibration postulated by Lei *et al.* (83) and advocated by Zecchina and coworkers (112). This assignment to υSi–O^- is also consistent with isotopic labeling studies of similar materials, which demonstrated that bands in the 1000- to 900-cm^{-1} region readily exhibit the expected redshift on substitution of ^{18}O for ^{16}O, but remained unaffected by deuteration (73, 90). Therefore, these Si–O^-G' groups are complementary to the Si(OG)Al structures and can account for at least some of the contribution to the additional band between 1000 and 900 cm^{-1} in the ion-exchanged samples. At low degrees of ion exchange, the majority of the Si(OG)Al and Si–O^-G' structures are likely to be present in isolated configurations that help maintain the copper ions in highly dispersed states, but as exchange levels approach and exceed 100%, a hybrid structure consisting of both groups may exist, as represented by Structure III in Fig. 13. When $G' = Cu^+$ and $G = Cu^+$ or H^+, the hybrid configuration of Structure III would appear as Structures IV and V, respectively, in Fig. 13. Structures I, IV, and V can maintain a highly dispersed form of Cu^+, which is located in close proximity to an Al tetrahedron bearing one negative charge. Structure VI, a four-member ring with tetrahedral Al at the $T9$ sites, can also maintain highly dispersed Cu ions. Indeed, it has been shown that Cu ions present at Al sites have drastically different adsorption properties compared with those located elsewhere (12, 14, 24, 26, 122). Reactant and product molecules must contact these structures

because they are located at the channel intersections created by the straight and zigzag 10-membered-ring pores through which the gases diffuse. Structure IV locates two Cu^+ ions near one another, thus accounting for part of the dimeric copper complexes often proposed as active sites for NO decomposition in Cu–ZSM-5 (11, 26, 27, 129).

For Cu–ZSM-5a, the transformation of the original 930-cm^{-1} band into the band near 965 cm^{-1} during the heating pretreatment and its reemergence after N_2O decomposition suggest a change in the oxidation state of these copper ions. Further evidence of redox behavior was provided by the replicated interchange of these two bands during repeated pretreatment/exposure cycles. Therefore, guided by the chemistry represented by Eqs. [1]–[7], it is reasonable to assign these two bands to Si–O^- stretching vibrations in the following structures: 930–910 cm^{-1}, Si–O^-G, with $G = [Cu^{2+}(H_2O)_{n-1}(OH^-)]^+$, $[Cu^{2+}(OH^-)]^+$, or $[Cu^{2+}(O^-)]^+$; and 975–965 cm^{-1}, Si–O^-Cu^+. The only apparent inconsistency with the latter assignment is the peak at 961 cm^{-1} for the as-received Cu–ZSM-5n. Zecchina and coworkers reported an initial band at 920 cm^{-1} for a Cu–ZSM-5 sample prepared with H–ZSM-5 (Si/Al = 14) by ion exchange with $Cu(NO_3)_2$ (112), and this strongly suggests that the nature of the precursor material has a significant effect on the initial position of this peak. Because these bands seem to depend strongly on the oxidation state of the *copper*, any associated ligands affect the wavenumber positions only to a limited extent. It is less clear how the presence of copper-containing groups affect the Si(O*G*)Al zeolite-related vibrations of Structure I (Fig. 13); regardless, if these assignments are applicable, then Si–O^-G' geometries must be present because the dominant IR changes for Cu–ZSM-5a during pretreatment and N_2O decomposition were in the 1000- to 900-cm^{-1} region.

As discussed previously, the bulky nature of the $[Cu^{2+}(H_2O)_{n-1}(OH^-)]^+$ complex and its $Cu^{2+}(H_2O)_n$ precursor retricts their location to the 10-membered-ring channel intersections. The Si–$O^-[Cu^{2+}(OH^-)]^+$ and Si–$O^-[Cu^{2+}(O^-)]^+$ configurations should be similarly positioned because they are initially created by sequential dehydration of $[Cu^{2+}(H_2O)_{n-1}(OH^-)]^+$ (Eqs. [3] and [6]). Thermal reduction of Cu^{2+} to Cu^+ is envisioned to occur through the Si–$O^-[Cu^{2+}(OH^-)]^+$ and Si–$O^-[Cu^{2+}(O^-)]^+$ structures (Eqs. [6] and [7]), thus the resulting Si–O^-Cu^+ entity also should be located at the 10-membered-ring channel intersections, but this does not exclude the Cu^+ from being in a recessed position, as suggested by Itho *et al.* (107). This sequence transforms the 930-cm^{-1} band into the 965-cm^{-1} band during thermal pretreatment of the Cu–ZSM-5a catalyst. Similar arguments support the assertion that the dispersed Si(O*G*)Al sites (Fig. 13, Structure I) are also located at the channel intersections, especially since these groups have already been claimed to be at this position (125, 126), but this restriction is less stringent in view of the proposed ability of the copper ions to migrate (107).

TABLE 3

N_2O Decomposition over Cu–ZSM-5 Catalysts at 623 K

Catalyst	P_{N_2O} (atm)	Activity ($\frac{\mu mol}{s \cdot g}$)	TOF (s^{-1})[a]	Ref.
3.7% Cu–ZSM-5a	0.99×10^{-3}	0.13	2.2×10^{-4}	5
4.6% Cu–ZSM-5n	1×10^{-3}[b]	0.35	4.8×10^{-4}	33

[a] Per Cu cation.

[b] Extrapolated using N_2O pressure dependence of 0.1.

In contrast to Cu–ZSM-5a, Cu–ZSM-5n originally displayed a band near 961 cm^{-1}, failed to show an identifiable peak for $[Cu^{2+}(OH^-)]^+$ in the 3700- to 3600-cm^{-1} region during pretreatment, and possessed a comparable amount of Brønsted acidity only at much higher pretreatment temperatures (Fig. 4). These points indicate that the Cu^{2+} ions exchanged into Cu–ZSM-5n were substantially different than those in Cu–ZSM-5a, and this is attributed to either the nonequivalent exchange materials, $Cu(NO_3)_2$ vs $Cu(OAc)_2$, or the different zeolite precursor, NH_4–ZSM-5 vs Na–ZSM-5. However, after the thermal pretreatment, bands between 1000 and 900 cm^{-1} were at nearly the same positions and comparable catalytic behavior during stoichiometric N_2O decomposition was obtained, as shown in Table 3. Li and Armor report a conversion at 623 K corresponding to a rate of 0.13 μmol of $N_2O \cdot s^{-1} \cdot g^{-1}$ with the Cu–ZSM-5a catalyst (5), whereas in our laboratory a rate of 0.35 μmol of $N_2O \cdot s^{-1} \cdot g^{-1}$ was obtained with the Cu–ZSM-5n catalyst after correcting to the same N_2O pressure of 10^{-3} atm (33). These results are in closer agreement when compared on a turnover frequency basis, as indicated in Table 3.

The Si(OH)Al Band

The Cu–ZSM-5 catalysts also displayed a peak near 3595 cm^{-1} that immediately decreased on exposure to N_2O at elevated temperatures, as shown in Fig. 5 for Cu–ZSM-5a. This band is assigned to the O–H stretching vibration in the Si(OH)Al groups depicted by Structure I in Fig. 13, with $G = H^+$ (or more accurately $H^{\delta+}$). A reasonable possibility is that the Al–O bond cleaves to produce an Al atom possessing its three customary bonds and generates an internal silanol group such as that associated with an absorbance near 3500 cm^{-1} in highly siliceous ZSM-5 (130). This can account for part of the increase in the υO–H region compared to that exhibited by Na–ZSM-5 in Fig. 2. Further support of this sequence is the postulate that this bridging can be represented by two equilibrium forms (69, 80):

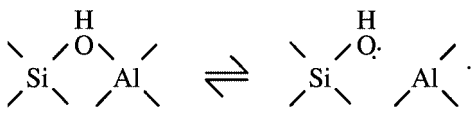

[8]

Normally, the position of this equilibrium lies far to the left,

but contact with N_2O could shift it to the right, particularly if adsorption occurred on Cu^+ sites, as depicted in Structure V (Fig. 13), because oxidation to Cu^{2+} would expose the bridging OH group to a more electropositive cation, which would have a stronger electron affinity.

As mentioned previously, CH_4 adsorption at 173 K on outgassed H–ZSM-5 caused a decrease in the band at 3622 cm^{-1} and led to the simultaneous appearance of hydroxyl bands at 3648 and 3510 cm^{-1}, with the latter strong band attributed to the 3622-cm^{-1} feature shifted as a result of the perturbation of surface-bridging hydroxyl groups by adsorbed CH_4 (113). This observation was offered as evidence for the interaction of CH_4 with OH groups of H–ZSM-5 and led these authors to conclude that Si(OH)Al bridging hydroxyl groups play an important role in CH_4 adsorption on that zeolite. In view of its polarizability in the axial direction, N_2O is a very soft base (47, 48) and would thus interact with only the strongest, and consequently least abundant, acid sites; however, such an interaction still would not be strong enough to result in the formation of $[N_2OH]^+$ because complete proton transfer reactions occur only when acidic OH groups react with very strong bases (21). Because H–ZSM-5 and H–USY zeolites are inactive for N_2O decomposition below 773 K, it has been concluded that any influence of acid sites on the rate of N_2O decomposition over Ru–ZSM-5 and Ru–HNaUSY catalysts must be due to interactions between protons and Ru cations and not to direct N_2O decomposition on Brønsted acid sites (131). This same conclusion should also apply to Cu–ZSM-5.

N_2O Decomposition on Cu–ZSM-5

N_2O decomposition may occur on any or all of the Cu^+ sites illustrated by Structures I–V in Fig. 13; however, certain sites could dominate the kinetics. For instance, IR-detectable changes which occurred rapidly after introducing N_2O, but before the detection of gas-phase O_2, could simply reflect the oxidation of spectator and/or less active copper species. It would seem that some special characteristic of the ZSM-5 structure, other than providing dispersed copper ions, must likely be invoked to explain why both a proper metal and a suitable support are required for the unique high activity of Cu–ZSM-5 for N_2O decomposition.

We propose that catalytically important chemistry occurs on copper ions at the $Si–O^-$ sites in Structure V, as depicted in Fig. 14. Gas-phase N_2O first adsorbs molecularly via the O end onto Cu^+ (Fig. 14A, Eq. [R1]). This step is consistent with the transient, but reproducible, increases in absorbance between 2225 and 2170 cm^{-1} in the presence of N_2O and is strongly preferred to N_2O adsorption via the N end to give $Cu^+–N_2O$, which has been claimed to be a spectator species on overexchanged Cu–ZSM-5 (32). This chemistry is also consistent with the postulate that N_2O preferentially adsorbs on Cu^+ associated with Si rather than Cu^+ associated with Al (32). Once adsorbed, N_2O dissociates irreversibly to generate gas-phase N_2 and adsorbed O (Fig. 14A, Eq. [R2(a)]), and this step involves the final cleavage of the Al–O bond to form an internal silanol group. This sequence of events involving Structure V sites: (a) results in the formation of $[Cu^{2+}(O^-)]^+$ by oxidation of Cu^+ to Cu^{2+}; (b) accounts for the decrease of the 3590 cm^{-1} band for Si(OH)Al as well as the increases of the 3500 and 915 cm^{-1} bands for internal Si–OH and $Si–O^-[Cu^{2+}(O^-)]^+$, respectively; (c) illustrates a means by which extralattice oxygen (ELO) is stabilized in the form of $[Cu^{2+}(O^-)]^+$; and (d) explains the delayed decrease in the 985- to 970-cm^{-1} region (compare Figs. 5c and 8a) whereby $Si–O^-Cu^+$ species are converted into $Si–O^-[Cu^{2+}(O^-)]^+$ groups (band at 910 cm^{-1}). The time needed to achieve this also allows a less stringent requirement regarding Al–O bond breakage. A slight variation of this step can be proposed (see Fig. 14A, Eq. [R2(b)]) to account for some of the enhanced absorbance near 3650 cm^{-1}, which has been assigned to the O–H stretching vibration of $[Cu^{2+}(OH^-)]^+$, the configuration in which the ELO would then be stabilized. Even though the sequences described by Eqs. [R2(a)] and [R2(b)] can occur to different extents, the former is preferred because it provides a relatively more stable zeolite configuration (Si–OH vs Si–O) and produces an N_2O-induced shift in the position of the Si(OH)Al equilibrium (Eq. [8]).

During the early stages of exposure, some fraction of the available Cu^+ sites remains unoccupied and interacts with the liberated N_2, a situation which can account for the appearance of the 2157-cm^{-1} band assigned to weakly sigma-bonded $Cu^+–N_2$. Any assignment of this band to $Cu^+–CO$ requires an adventitious source of CO, such as a CO impurity in the feed gases or partial oxidation of carbon impurities, but this was extremely unlikely, especially with Cu–ZSM-5n. As the Cu^+ sites become more completely oxidized, fewer free Cu^+ sites remain, and this transition from Cu^+ to Cu^{2+} leads to the eventual inability to detect any absorbance for the 2157-cm^{-1} band. When the copper becomes sufficiently oxidized, reaction of adsorbed N_2O with the O atom in the Cu coordination sphere results in the formation of N_2 and O_2, the simultaneous reduction of Cu^{2+} to Cu^+, as depicted by Eq. [R3(a)] (Fig. 14A), and the regeneration of the preferred catalytic site without any degradation to the framework. Eq. [R3(b)] (Fig. 14A) provides an explanation for the inability to recover the catalyst IR spectrum as it existed immediately prior to N_2O exposure. The irreversible steps illustrated in Eqs. [R3(a)] and [R3(b)] cannot account for the inhibitory effect of O_2 on the reaction rate observed for Cu–ZSM-5n (33); thus a reasonable alternative is the proposal that two of the sites on the right-hand-side of either Eq. [R2(a)] or [R2(b)] are neighbors so that the ELO from either $[Cu^{2+}(O^-)]^+$ or $[Cu^{2+}(OH^-)]^+$ can recombine to form O_2, as show in Fig. 14B, Eq. [R4(a)] or [R4(b)]. Recent work by Bell and coworkers (132) indicates that in ZSM-5 the fraction of Al atoms having

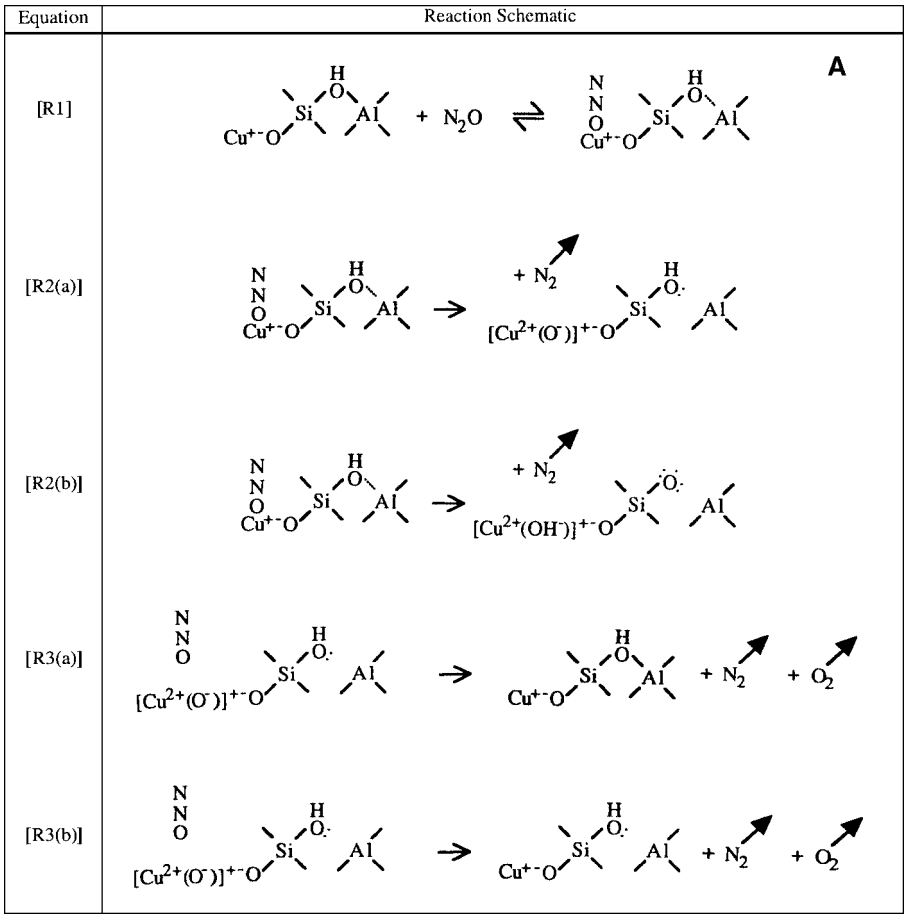

FIG. 14. Proposed reaction chemistry to describe N_2O decomposition on Cu–ZSM-5 involving Structures V and VI (see Fig. 13 and text).

another Al in next nearest neighbor (NNN) *T* sites is 0.64 for a Si/Al ratio of 12 and is estimated to be ~0.58 for a Si/Al ratio of 14. Based on these results, at least 50% of the Al *T* sites in the Cu–ZSM-5a and Cu–ZSM-5n catalysts should have another Al as a NNN, and at least some of these site pairs could allow for O_2 formation in this manner. These NNN Al atoms can be either in different rings, as in Eqs. [R4(a)] and [R4(b)], or in the same ring. The ZSM-5 structure can provide a four-membered-ring configuration (see Structure VI in Fig. 13) that is essentially equivalent to two Structure V geometries joined through O linkages with Al situated at the *T*9 sites. The same N_2O decomposition chemistry is proposed to occur on isolated Structure V groups, as outlined in Figs. 14A and 14B by Eqs. [R1]–[R4], until a four-membered ring is attained with one of the configurations in Fig. 14B, Eq. [R5], with equilibrium favoring the left-hand-side given the presumed stability of Si–OH over that of Si–O; however, with two dangling Si–O bonds in close proximity, the structure on the right-hand-side could result in recombination and O_2 formation from oxygen originally bound to the lattice, as shown in Fig. 14B, Eq. [R6]. The observation that desorbed O_2 initially contained lattice oxygen exclusively during NO decomposition serves as the basis for this supposition even though there is no direct evidence for similar behavior for N_2O decomposition on Cu–ZSM-5, but this characteristic was indeed witnessed using Fe–MOR (133). The lone electrons associated with the Si atoms produce a charge imbalance that either could be moderated by delocalization over the collective copper/zeolite system or could facilitate reduction whereby the ELO deposited in the form of $[Cu^{2+}(OH^-)]^+$ enters the site originally containing lattice oxygen to reform a bridging hydroxyl group while simultaneously reducing Cu^{2+} to Cu^+, as illustrated in Fig. 14C, Eq. [R7]. The formation of bridging hydroxyl groups instead of internal silanols is favored from stability considerations. These redox cycles can continue until all of the original lattice-bound oxygen would be replaced by O atoms initially contained in N_2O.

A ZSM-5 unit cell contains 96 tetrahedral *T* sites (T = Si or Al) comprising 25 unique rings among a total of 168 rings, of which four (or 2.4%) are four-membered rings (132). At a Si/Al ratio of 12, the fraction of four-membered rings having two Al atoms is 0.014, and at a ratio of 14, the fraction of four-membered rings possessing two Al atoms is

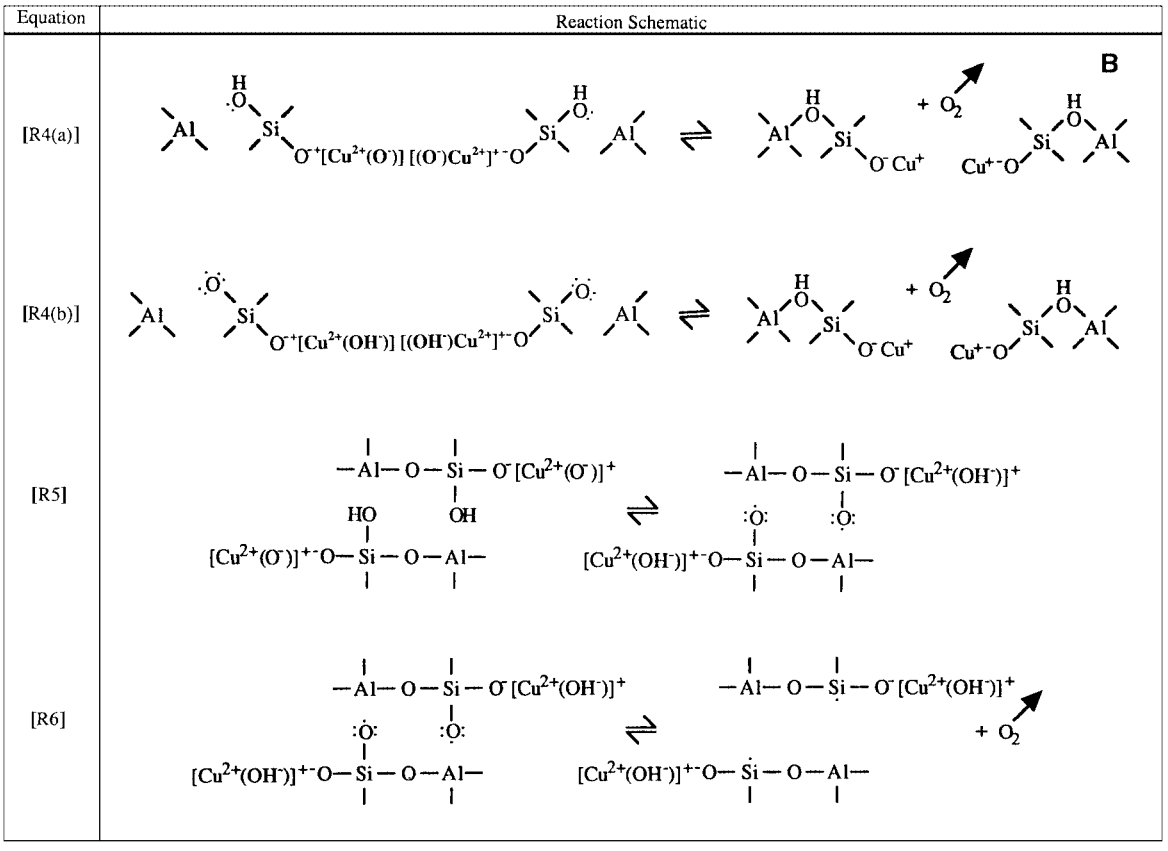

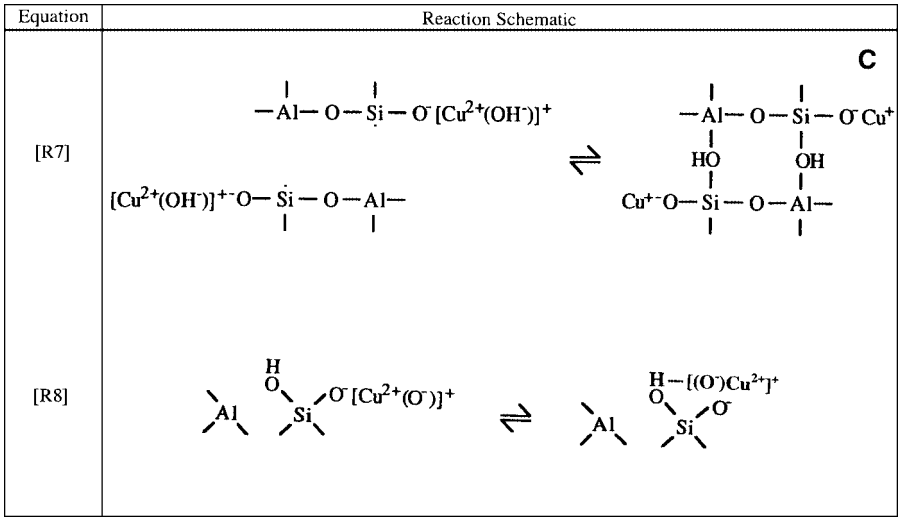

FIG. 14—*Continued*

estimated to be about 0.01 (132). Thus, if the majority of the catalytic activity occurred at these locations, they would represent a relatively small number of highly active sites, which would be formed during "overexchange" of Cu^{2+}, and this would account for the large increase in activity as the catalysts transition from being less than fully exchanged to being overexchanged (31, 32). If these four-membered-ring structures controlled the reactivity, then deactivation of these sites (by steam-induced dealumination, for example) would result in a substantial decrease in N_2O decomposition activity without significant degradation of the macroscopic zeolite structure. When Cu–ZSM-5 was used as a lean NO_x reduction catalyst, no gross destruction of the zeolite framework was detected, even after 50% deactivation (22). A band at 3450 cm^{-1} in H-boralites (isomorphically substituted B-containing zeolites) has been assigned to

Si–OH–O hydroxy groups bonded by a strong *intramolecular* hydrogen bond (134). This concept can be extended to Cu–ZSM-5 N_2O decomposition catalysts by envisioning that a suitably positioned internal Si–OH group forms a hydrogen bond with the ELO of the $Si–O^-[Cu^{2+}(O^-)]^+$ species, as depicted in Fig. 14C, Eq. R8, with the right-hand structure being intermediate on the way to the formation of $Si–O^-[Cu^{2+}(OH^-)]^+$ (Figs. 14A and 14B, Eqs.[R2(b)] and [R5]). The delayed reactivity of the Structure V and VI sites (Fig. 13) implies that they are less stable toward oxidation than those of other configurations; consequently, they should be more readily reduced once N_2O is removed. Indeed, as seen in Fig. 10b, purging N_2O with Ar at 643 K increased the 973-cm^{-1} peak assigned to $Si–O^-Cu^+$ and decreased the 928-cm^{-1} band assigned to $Si–O^-[Cu^{2+}(O^-)]^+$. Comparable trends were observed when Cu–ZSM-5a was contacted with CO at 673 K after exposure to N_2O and, in addition, the υO–H region in Fig. 12a exhibits changes opposite to those under oxidizing (N_2O or O_2) conditions, further supporting reversible redox chemistry.

The catalytic sequence depicted by the steps in Fig. 14 can be easily represented by simple Langmuir–Hinshelwood kinetics, i.e.,

$$2\left[N_2O + S \overset{K_{N_2O}}{\rightleftharpoons} N_2O–S\right], \quad [9]$$

$$2\left[N_2O–S \overset{k_3}{\rightarrow} N_2 + O–S\right] \quad \text{(rds)}, \quad [10]$$

$$2S–O \underset{k_{-3}}{\overset{k_3}{\rightleftharpoons}} O_2 + 2S, \quad [11]$$

$$2N_2O \rightarrow 2N_2 + O_2,$$

where S is an active site such as Structure V. This sequence with the first and last steps quasiequilibrated and the second a rate-determining step was proposed earlier for Cu–ZSM-5 (31, 33), and it gives the rate expression below, where L represents the total number of active sites and $K_{O_2} = k_{-3}/k_3$:

$$r = \frac{Lk_2K_{N_2O}P_{N_2O}}{1 + K_{N_2O}P_{N_2O} + K_{O_2}^{0.5}P_{O_2}^{0.5}}. \quad [12]$$

Dandekar and Vannice reported empirical reaction orders of 0.08–0.31 for N_2O and -0.07 to -0.31 for O_2 with Cu–ZSM-5n (33), values that can be approximated by Eq. [12] over specific pressure ranges. This equation also provided an excellent fit to experimental rate data obtained for Cu–ZSM-5n between 623 and 673 K along with thermodynamically consistent enthalpies and entropies of adsorption for N_2O and O_2 (33).

Debate currently exists regarding details of the NO decomposition reaction, and it has been proposed to occur on single Cu^+ sites by first forming a mononitrosyl species followed by a gem–dinitrosyl species which then decomposes into N_2O and leaves an adsorbed O atom, which, in the process, oxidizes Cu^+ to Cu^{2+} (135). Consequently, the first steps of NO decomposition have been represented as follows (28):

$$Cu^+(NO) \underset{-NO}{\overset{+NO}{\rightleftharpoons}} Cu^+\begin{matrix}\diagup NO \\ \diagdown NO\end{matrix} \rightarrow Cu^{2+}\begin{matrix}\diagup O^- \\ \diagdown N_2O\end{matrix}. \quad [13]$$

Structure VII

Not only does the resulting intermediate, Structure VII, contain the $[Cu^{2+}(O)^-]^+$ species that has been associated with the band near 930 cm^{-1}, but the claimed instability of this structure under reaction conditions provides a means by which NO displaces N_2O in the gas phase. Hence, various key features postulated in this paper to describe N_2O decomposition could also pertain to NO decomposition and could offer other alternative routes to describe NO decomposition over Cu–ZSM-5 catalysts.

SUMMARY

The decomposition of N_2O over Cu–ZSM-5 catalysts was studied using DRIFTS. In addition to the IR bands exhibited by Na–ZSM-5, the room-temperature spectra of Cu–ZSM-5 prior to any thermal treatment displayed an additional band between 1000 and 900 cm^{-1}, which was assigned to the stretching mode of an $Si–O^-$ bond perturbed by Cu^{2+} species as opposed to a Cu-perturbed zeolite vibration. Purging in Ar at 300 K removed both adsorbed water and water coordinated in octahedral $[Cu(H_2O)_6]^{2+}$ complexes from the zeolite material. Heating to 773 K resulted in the thermal reduction of Cu^{2+} to Cu^+, and a substantial fraction of the copper ions was stabilized as $Si–O^-Cu^+$. During the introduction of N_2O to Cu–ZSM-5, transient bands were observed which were assigned to adsorbed N_2O bonded via the O atom. Only Cu–ZSM-5 exhibited a slight, but rapid, decrease in the 3597 cm^{-1} υOH band for bridging Si(OH)Al groups, and this was accompanied by the appearance of a band near 910 cm^{-1}, indicating oxidation of Cu^+ to Cu^{2+}. No unequivocal bands for adsorbed N_2O were detected under steady-state decomposition conditions with any of the catalysts, indicating very low steady-state surface concentrations of adsorbed N_2O.

These DRIFTS results are consistent with a proposed redox mechanism describing N_2O decomposition over Cu–ZSM-5. Gas-phase N_2O adsorbs molecularly via the O end onto the Cu^+ ion at a $Si–O^-Cu^+$ site maintained in a highly dispersed state. This adsorbed N_2O species then irreversibly decomposes to form gaseous N_2 and an adsorbed O atom, and in the process Cu^+ is oxidized to Cu^{2+}, which is stabilized as $Si–O^-[Cu^{2+}(O^-)]^+$ or $Si–O^-[Cu^{2+}(OH^-)]^+$. When two such sites are located in close proximity, such as at opposite corners of a four-membered ring having Al tetrahedra at the $T9$ sites of the ZSM-5 zeolite, oxygen recombination can readily occur to form O_2 and in the process Cu^{2+} is

reduced to Cu^+, thus completing the catalytic redox cycle. This mechanism incorporates aspects of both the copper ion and the zeolite structure to account for the uniquely high activity of this particular catalyst.

ACKNOWLEDGMENT

This study was sponsored by Air Products & Chemicals, Inc.

REFERENCES

1. Swamy, C. S., and Christopher, J., *Catal. Rev.–Sci. Eng*. **34**, 409 (1992).
2. Kung, H. H., "Transition Metal Oxides: Surface Chemistry and Catalysis." Elsevier, Amsterdam, 1989.
3. Luys, M.-J., van Oeffelt, P. H., Pieters, P., and Ter Veen, R., *Catal. Today* **10**, 283 (1991).
4. Barin, I., "Thermochemical Data of Pure Substances. Part I: Ag-Kr," 2nd ed. VCH, Weinheim/New York, 1993.
5. Li, Y., and Armor, J. N., *Appl. Catal. B* **1**, L21 (1992).
6. Li, Y., and Armor, J. N., U.S. Patent 5, 171, 553 (1992).
7. Iwamoto, M., Furukawa, H., and Kagawa, S., *in* "New Developments in Zeolite Science and Technology" (Y. Murakami, A. Lijima, and J. W. Ward, Eds.), p. 943. Elsevier, Amsterdam, 1986.
8. Iwamoto, M., Yahiro, H., Tanda, K., Mizuno, N., Mine, Y., and Kagawa, S., *J. Phys. Chem*. **95**, 3727 (1991).
9. Iwamoto, M., Yahiro, H., Mizuno, N., Zhang, W.-X., Mine, Y., Furukawa, H., and Kagawa, S., *J. Phys. Chem*. **96**, 9360 (1992).
10. Konduru, M. V., and Chuang, S. S. C., *J. Catal*. **187**, 436 (1999).
11. Kucherov, A. V., Shigapov, A. N., Ivanov, A. A., and Shelef, M., *J. Catal*. **186**, 334 (1999).
12. Millar, G. J., Canning, A., Rose, G., Wood, B., Trewartha, L., and Mackinnon, I. D. R., *J. Catal*. **183**, 169 (1999).
13. Carl, P. J., and Larsen, S. C., *J. Catal*. **182**, 208 (1999).
14. Wichterlová, B., Dědeček, J., Sobalík, Z., Vondrová, A., and Klier, K., *J. Catal*. **169**, 194 (1997).
15. Chang, Y.-F., and McCarty, J. G., *J. Catal*. **165**, 1 (1997).
16. Pirone, R., Garufi, E., Ciambelli, P., Moretti, G., and Russo, G., *Catal. Lett*. **43**, 255 (1997).
17. Curtin, T., Grange, P., and Delmon, B., *Catal. Today* **35**, 121 (1997).
18. Wang, Z., Sklyarov, A. V., and Keulks, G. W., *Catal. Today* **33**, 291 (1997).
19. Yan, J. Y., Sachtler, W. M. H., and Kung, H. H., *Catal. Today* **33**, 279 (1997).
20. Hwang, I. C., and Woo, S. I., *J. Phys. Chem. B* **101**, 4055 (1997).
21. Szanyi, J., and Paffett, M. T., *J. Catal*. **164**, 232 (1996).
22. Yan, J. Y., Lei, G.-D., Sachtler, W. M. H., and Kung, H. H., *J. Catal*. **161**, 43 (1996).
23. Cheung, T., Bhargava, S. K., Hobday, M., and Foger, K., *J. Catal*. **158**, 301 (1996).
24. Wichterlová, B., Sobalík, Z., and Vondrová, A., *Catal. Today* **29**, 149 (1996).
25. Aylor, A. W., Larsen, S. C., Reimer, J. A., and Bell, A. T., *J. Catal*. **157**, 592 (1995).
26. Dědeček, J., Sobalik, Z., Tvarůžková, Z., Kaucký, D., and Wichterlová, B., *J. Phys. Chem*. **99**, 16327 (1995).
27. Shelef, M., *Chem. Rev*. **95**, 209 (1995).
28. Spoto, G., Zecchina, A., Bordiga, S., Ricchiardi, G., Martra, G., Leofanti, G., and Petrini, G., *Appl. Catal. B* **3**, 151 (1994).
29. Thiemens, M. H., and Trogler, W. C., *Science* **251**, 932 (1991).
30. Riley, B. W., and Richmond, J. R., *Catal. Today* **17**, 277 (1993).
31. Kapteijn, F., Rodriguez-Mirasol, J., and Moulijn, J. A., *Appl. Catal. B* **9**, 25 (1996).
32. Konduru, M. V., and Chuang, S. S. C., *J. Catal*. **196**, 271 (2000).
33. Dandekar, A., and Vannice, M. A., *Appl. Catal. B* **22**, 179 (1999).
34. Ciambelli, P., Di Benedetto, A., Garufi, E., Pirone, R., and Russo, G., *J. Catal*. **175**, 161 (1998).
35. Pophal, C., Yogo, T., Tanabe, K., and Segawa, K., *Catal. Lett*. **44**, 271 (1997).
36. Imamura, S., Kitao, T., Kanai, H., Shono, S., Utani, K., and Jindai, H., *React. Kinet. Catal. Lett*. **61**, 201 (1997).
37. Kapteijn, F., Marbán, G., Rodriguez-Mirasol, J., and Moulijn, J. A., *J. Catal*. **167**, 256 (1997).
38. Turek, T., *Appl. Catal. B* **9**, 201 (1996).
39. Montes de Correa, C., Villa, A. L., and Zapata, M., *Catal. Lett*. **38**, 27 (1996).
40. Kapteijn, F., Mul, G., Marbán, G., Rodriguez-Mirasol, J., and Moulijn, J. A., *in* "Proceedings, 11th International Congress on Catalysis Baltimore, 1996" (J. W. Hightower, W. N. Delgass, E. Iglesia, and A. T. Bell, Eds.), Vol. 101, p. 641. Elsevier, Amsterdam, 1996.
41. Lin, J., Chen, H. Y., Chen, L., Tan, K. L., and Zeng, H. C., *Appl. Surf. Sci*. **103**, 307 (1996).
42. Morterra, C., Giamello, E., Cerrato, G., Centi, G., and Perathoner, S., *J. Catal*. **179**, 111 (1998).
43. Yao, K.-W., Jaenicke, S., Lin, J.-Y., and Tan, K. L., *Appl. Catal. B* **16**, 291 (1998).
44. Centi, G., Dall'Olio, L., and Perathoner, S., *J. Catal*. **192**, 224 (2000).
45. Centi, G., Dall'Olio, L., and Perathoner, S., *J. Catal*. **194**, 130 (2000).
46. Hussain, G., Rahman, M. M., and Sheppard, N., *Spectrochim. Acta* **47A**, 1525 (1991).
47. Morterra, C., Boccuzzi, F., Coluccia, S., and Ghiotti, G., *J. Catal*. **65**, 231 (1980).
48. Borello, E., Cerruti, L., Ghiotti, G., and Guglielminotti, E., *Inorg. Chim. Acta* **6**, 45 (1972).
49. Forster, H., and Remmert, M., *J. Mol. Struct*. **174**, 357 (1988).
50. Nogin, A. V., Alekseev, A. V., and Filimonov, V. N., *Russ. J. Phys. Chem*. **50**, 99 (1976).
51. Busca, G., and Lorenzelli, V., *J. Catal*. **72**, 303 (1981).
52. Dalla Betta, R. A., Garten, R. L., and Boudart, M., *J. Catal*. **41**, 40 (1976).
53. Sano, T., Negishi, N., Mas, D., and Takeuchi, K., *J. Catal*. **194**, 71 (2000).
54. Ebitani, K., Morokuma, M., Kim, J.-H., and Morikawa, A., *J. Chem. Soc. Faraday Trans*. **90**, 377 (1994).
55. Ebitani, K., Morokuma, M., Kim, J.-H., and Morikawa, A., *J. Catal*. **141**, 725 (1993).
56. Zholobenko, V., *J. Chem. Soc. Mendeleev Commun*. 67 (1993).
57. Zholobenko, V. L., Kustov, L. M., and Kazansky, V. B., *in* "Proceedings, 9th International Zeolite Conference" (R. von Ballmoos, *et al.*, Eds.), p. 299. Buttersworth-Heinemann, Boston, MA, 1992.
58. Sobolev, V. I., Kharitonov, A. S., and Panov, G. I., *Doklady Phys. Chem*. **307**, 700 (1989).
59. Li, Y., and Armor, J. N., *Appl. Catal*. **76**, L1 (1991).
60. Li, Y., and Armor, J. N., *Appl. Catal. B* **3**, 55 (1993).
61. Fanning, P. E., Ph.D. thesis. Pennsylvania State University, University Park, PA, 1996.
62. Fanning, P. E., and Vannice, M. A., *Carbon* **31**, 721 (1993).
63. Venter, J. J., and Vannice, M. A., *Appl. Spectrosc*. **42**, 1096 (1988).
64. Venter, J. J., and Vannice, M. A., *Carbon* **26**, 889 (1988).
65. Zhdanov, S. P., Kosheleva, L. S., and Titova, T. I., *Doklady Phys. Chem*. **303**, 1132 (1988).
66. Benesi, H. A., and Jones, A. C., *J. Phys. Chem*. **63**, 179 (1959).
67. Fink, P., and Datka, J., *J. Chem. Soc. Faraday Trans. 1* **85**, 3079 (1989).
68. Szostak, R., "Handbook of Molecular Sieves." Van Nostrand Reinhold, New York, 1992.
69. Szostak, R., "Molecular Sieves: Principles of Synthesis and Identification." Van Nostrand Reinhold, New York, 1989.

70. Coudurier, G., Naccache, C., and Vedrine, J. C., *J. Chem. Soc. Chem. Commun*. 1413 (1982).
71. Jansen, J. C., van der Gaag, F. J., and van Bekkum, H., *Zeolites* **4**, 369 (1984).
72. Flanigen, E. M., Khatami, H., and Szymanski, H. A., *Adv. Chem.* **101** p. 201 (1971).
73. Valyon, J., and Hall, W. K., *J. Phys. Chem*. **97**, 7054 (1993).
74. Sárkány, J., and Sachtler, W. M. H., *Zeolites* **14**, 7 (1994).
75. Sárkány, J., d'Itri, J. L., and Sachtler, W. M. H., *Catal. Lett*. **16**, 241 (1992).
76. Li, Y., and Armor, J. N., *J. Catal*. **145**, 1 (1994).
77. Anpo, M., Matsuoka, M., Shioya, Y., Yamashita, H., Giamello, E., Morterra, C., Che, M., Patterson, H. H., Webber, S., Ouellette, S., and Fox, M. A., *J. Phys. Chem*. **98**, 5744 (1994).
78. Heitmann, G. P., Dahlhoff, G., Niederer, J. P. M., and Hölderich, W. F., *J. Catal*. **194**, 122 (2000).
79. Chu, C. T-W., and Chang, C. D., *J. Phys. Chem*. **89**, 1569 (1985).
80. Haag, W. O., Lago, R. M., and Weisz, P. B., *Nature* **309**, 589 (1984).
81. Neyman, K. M., Strodel, P., Ruzankin, S. Ph., Schlensog, N., Knözinger, H., and Rösch, N., *Catal. Lett*. **31**, 273 (1995).
82. Romotowski, T., Komorek, J., Paukshtis, Ye. A., and Yurchenko, E. N., *Zeolites* **11**, 497 (1991).
83. Lei, G. D., Adelman, B. J., Sárkány, J., and Sachtler, W. M. H., *Appl. Catal. B* **5**, 245 (1995).
84. Diaz, G., Perez-Hernandez, R., Gomez-Cortes, A., Benaissa, M., Mariscal, R., and Fierro, J. L. G., *J. Catal*. **187**, 1 (1999).
85. Camblor, M. A., Corma, A., and Pérez-Pariente, J., *J. Chem. Soc. Chem. Commun*. 557 (1993).
86. Notari, B., *in* "Symposium on New Catalytic Chemistry Utilizing Molecular Sieves, 206th National Meeting of the ACS," p. 761. Am. Chem. Soc., Washington, DC, 1993.
87. Decottignies, M., Phalippou, J., and Zarzycki, J., *J. Mater. Sci*. **13**, 2605 (1978).
88. Duran, A., Serna, C., Fornes, V., and Fernandez Navarro, J. M., *J. Non-Cryst. Solids* **82**, 69 (1986).
89. Boccuzzi, F., Coluccia, S., Ghiotti, G., Morterra, C., and Zecchina, A., *J. Phys. Chem*. **82**, 1298 (1978).
90. Hino, M., and Sato, T., *Bull. Chem. Soc. Jpn*. **44**, 33 (1971).
91. Ocaña, M., Fornés, V., and Serna, C. J., *J. Non-Cryst. Solids* **107**, 187 (1989).
92. White, R. L., and Nair, A., *Appl. Spectrosc*. **44**, 69 (1990).
93. Baraldi, P., and Fabbri, G., *Spectrochim. Acta* **37A**, 89 (1981).
94. Vratny, F., Rao, C. N. R., and Dilling, M., *Anal. Chem*. **33**, 1455 (1961).
95. Heyns, A. M., *J. Mol. Struct*. **11**, 93 (1972).
96. Socrates, G., "Infrared Characteristic Group Frequencies," 2nd ed. Wiley, Chichester, 1994.
97. Nakamoto, K., "Infrared and Raman Spectra of Inorganic and Coordination Compounds," 4th ed. Wiley, New York, 1986.
98. Nakamoto, K., "Infrared and Raman Spectra of Inorganic and Coordination Compounds," 3rd ed. Wiley, New York, 1978.
99. Védrine, J. C., Auroux, A., Bolis, V., Dejaifve, P., Naccache, C., Wierzchowski, P., Derouane, E. G., Nagy, J. B., Gilson, J.-P., van Hooff, J. H. C., van den Berg, J. P., and Wolthuizen, J., *J. Catal*. **59**, 248 (1979).
100. Parker, L. M., Bibby, D. M., and Burns, G. R., *Zeolites* **13**, 107 (1993).
101. Pouchert, C. J., Ed., "The Aldrich Library of FT-IR Spectra: Vapor Phase." Aldrich Chem. Co., Milwaukee, WI, 1989.
102. Carver, C. D., Ed., "Gases and Vapors." Coblentz Soc., The Society, Kirkwood, MO, 1980.
103. "The Sadtler Prism Standard Infrared Spectra, 1141." Sadtler Res. Lab., Philadelphia, PA, 1966.
104. "The Sadtler Prism Standard Infrared Spectra, 10559." Sadtler Res. Lab. Philadelphia, PA, 1966.
105. Huang, Y.-Y., *J. Am. Chem. Soc*. **95**, 6636 (1973).
106. Huang, Y.-Y., *J. Catal*. **30**, 187 (1973).
107. Itho, Y., Nishiyama, S., Tsuruya, S., and Masai, M., *J. Phys. Chem*., **98**, 960 (1994).
108. Chajar, Z., Primet, M., Praliaud, H., Chevrier, M., Gauthier, C., and Mathis, F., *Appl. Catal. B* **4**, 199 (1994).
109. Larsen, S. C., Aylor, A., Bell, A. T., and Reimer, J. A., *J. Phys. Chem*. **98**, 11533 (1994).
110. Centi, G., Perathoner, S., Shioya, Y., and Anpo, M., *Res. Chem. Intermed*. **17**, 125 (1992).
111. Jacobs, P. A., De Wilde, W., Schoonheydt, R. A., Uytterhoeven, J. B., and Beyer, H., *J. Chem. Soc., Faraday Trans. 1* **72**, 1221 (1976).
112. Turnes Palomino, G., Fisicaro, P., Giamello, E., Bordiga, S., Lamberti, C., and Zecchina, A., *J. Phys. Chem. B* **104**, 4064 (2000).
113. Chen, L., Lin, L., Xu, Z., Zhang, T., Xin, Q., Ying, P., Li, G., and Li, C., *J. Catal*. **161**, 107 (1996).
114. Valyon, J., and Hall, W. K., *J. Phys. Chem*. **97**, 1204 (1993).
115. Lokhov, Yu. A., and Davydov, A. A., *React. Kinet. Catal. Lett*. **3**, 39 (1975).
116. Davydov, A. A., and Lokhov, Yu. A., *React. Kinet. Catal. Lett*. **8**, 47 (1978).
117. Spoto, G., Bordiga, S., Ricchiardi, G., Scarano, D., and Zecchina, A., *J. Chem. Soc., Faraday Trans*. **91**, 3285 (1995).
118. Lamberti, C., Bordiga, S., Salvalaggio, M., Spoto, G., Zecchina, A., Geobaldo, F., Vlaic, G., and Bellatreccia, M., *J. Phys. Chem. B* **101**, 344 (1997).
119. Kuroda, Y., Konno, S.-I., Morimoto, K., and Yoshikawa, Y., *J. Chem. Soc. Chem. Commun*. 18 (1993).
120. Bell, V. A., Feeley, J. S., Deeba, M., and Farrauto, R. J., *Catal. Lett*. **29**, 15 (1994).
121. Anderson, M. W., and Kevan, L., *J. Phys. Chem*. **91**, 4174 (1987).
122. Parrillo, D. J., Dolenec, D., Gorte, R. J., and McCabe, R. W., *J. Catal*. **142**, 708 (1993).
123. Kuroda, Y., Kotani, A., Maeda, H., Moriwaki, H., Morimato, T., and Nagao, M., *J. Chem. Soc., Faraday Trans*. **88**, 1583 (1992).
124. Dzwigaj, S., Haber, J., and Romotowski, T., *Zeolites* **3**, 134 (1983).
125. Jacobs, P. A., and von Ballmoos, R., *J. Phys. Chem*. **86**, 3050 (1982).
126. Topsøe, N.-Y., Pedersen, K., and Derouane, E. G., *J. Catal*. **70**, 41 (1981).
127. Valyon, J., and Hall, W. K., *Catal. Lett*. **19**, 109 (1993).
128. Boccuti, M. R., Rao, K. M., Zecchina, A., Leofanti, G., and Petrini, G., *in* "Structure and Reactivity of Surfaces" (C. Morterra, A. Zecchina, and G. Costa, Eds.), p. 133. Elsevier, Amsterdam, 1989.
129. Moretti, G., *Catal. Lett*. **28**, 143 (1994).
130. Woolery, G. L., Alemany, L. B., Dessau, R. M., and Chester, A. W., *Zeolites* **6**, 14 (1986).
131. Chang, Y.-F., McCarty, J. G., Wachsman, E. D., and Wong, V. L., *Appl. Catal. B* **4**, 283 (1994).
132. Rice, M. J., Chakraborty, A. K., and Bell, A. T., *J. Catal*. **186**, 222 (1999).
133. Valyon, J., Millman, W. S., and Hall, W. K., *Catal. Lett*. **24**, 215 (1994).
134. Datka, J., and Kawalek, M. *J. Chem. Soc., Faraday Trans*. **89**, 1829 (1993).
135. Hall, W. K, and Valyon, J., *Catal. Lett*. **15**, 311 (1992).